nature portfolio

Peer Review File

Full-course NIR-II imaging-navigated fractionated photodynamic therapy of bladder tumours with X-ray-activated nanotransducers



Open Access This file is licensed under a Creative Commons Attribution 4.0 International License, which permits use, sharing, adaptation, distribution and reproduction in any medium or format, as long as you give appropriate credit to the original author(s) and the source, provide a link to the Creative Commons license, and indicate if changes were made. In the cases where the authors are anonymous, such as is the case for the reports of anonymous peer reviewers, author attribution should be to 'Anonymous Referee' followed by a clear attribution to the source work. The images or other third party material in this file are included in the article's Creative Commons license, unless indicated otherwise in a credit line to the material. If material is not included in the article's Creative Commons license and your intended use is not permitted by statutory regulation or exceeds the permitted use, you will need to obtain permission directly from the copyright holder. To view a copy of this license, visit http://creativecommons.org/licenses/by/4.0/.

REVIEWER COMMENTS

Reviewer #1 (Luminescent nanomaterials, NPs):

He et al report the use of lanthanide nanoparticles activated by X-rays for imaging in NIR-II an photodynamic applications in a murine bladder tumor model.
The manuscript is well written and the work is of interest to the audience of Nat Comm, and should be published after minor recommendations.
The reviewer has some comments:
- with ref 22-25 the authors should also add this: Light: Science & Applications (2022) 11:123, doi.org/10.1038/s41377-022-00808-6
- do the authors have an idea of the quantity of AEP grafted on the nanoparticles? If not which technique could be used?
- do the authors know how this molecule is grafted on the nanoparticles?
- in Fig 2d, the authors show the size of NS measured by DLS after the different coating steps. The size is quite large compared to initial ~25 nm measured by TEM. How do they explain this large increase?
- for the grafting of FITC on NS, the authors used EDC/NHS. What is their role?
- the authors used a FITC-RGD peptide. What is the role of using a FITC peptide if the NS is already labelled?
- do the authors have an idea of the amount of peptide grafted on the NS? If not which technique could be used to determine this amount?
- are the nanoparticles stable in injection medium?
- how many nanoparticles are injected?

Reviewer #2 (NIR, molecular imaging):

The authors developed non-invasive fractionated photodynamic therapy (f-PDT) of bladder cancer with full-course real-time NIR-II imaging based on engineered X-ray-activated nanotransducers that contain lanthanide-doped nanoscintillators with concurrent emissions in visible and the second near-infrared (NIR-II) regions and conjugated photosensitizers. This is an interesting study, but there are several issues needed to addressed before further consideration.

1. The authors claim that the hexagonal Ln-NSs exhibit more intense X-ray-activated green and NIR-II radioluminescence than the rod-shaped Ln-NSs with anisotropic epitaxial growth. Why would this happen? The mechanism of this phenomenon need to be further explained.
2. What is the reason for the change in Zeta potential from +8.9 eV for NSs-AEP and +21.5 eV for NSs-RB to -40.3 eV for NSs-RB-cRGD? Is it the reason for the introduction of cRGD? Authors should explain it in detail.
3. The authors used infused imaging to verify the targeting of NSs-RB-cRGD, but there are certain problems in the current study. First, the authors did not verify the expression of αvβ3 in tumors and normal tissues in the induction model. Second, imaging validations of different tumor cell lines with high and low αvβ3 expression are also necessary to demonstrate the targeted uptake ability of NSs-RB-cRGD.

Third, as can be seen in Figure 2b, the induced tumor lesions are diffusely distributed, while in the fluorescence images in Figure 2f, the fluorescence distribution is a single bright spot. The fluorescence pattern of the non-diffuse distribution may be caused by infused residue or non-specific adsorption. It is recommended that the authors supplement more relevant and solid results to prove the specificity.
4. The authors proposed that nanoscintillators play an important role in the generation of cytotoxic hydroxyl radicals (· OH), whether there is further theoretical support and data validation?
5. Does tumor necrosis induced by radiotherapy/photodynamic therapy affect tumor uptake of the probe and thus the fluorescence signal? If so, does this introduce additional errors in the therapeutic effect evaluation given by the NIR-II fluorescence imaging?
6. The authors claim that the whole process of non-invasive real-time NIR-II imaging and on-demand use of f-PDT are reliable. However, the treatment effect of this method is not compared with the traditional invasive treatment effect. The superiority of the proposed treatment effect should be further verified.

Reviewer #3 (nanomedicine, cancer therapy):

I didn't have much time, but I think the manuscript/paper has potential. It's much too dense in its current format. Restructuring and focusing on the main findings in the main manuscript would really help.

Reviewer #4 (cancer imaging, clinical):

Reviewer summary: The authors synthesize novel nanotransducers that can be activated by x-ray or laser to emit in the visible and near-infrared regions. These nanotransducers are conjugated with peptides that specifically bind to tumor cells. Following activation by external x-rays, these compounds result in increased tumor cell killing and improved survival of mice bearing NMIBC tumors. Using infrared imaging, tumors can be non-invasively monitored after treatment.

The work addresses a significant clinical problem, as NMIBC is common and frequently recurs following treatment. Furthermore, disease monitoring currently requires cystoscopy/biopsy, which is invasive and is imperfect at estimating disease burden and extent. On the technical side, I have some significant questions and potential concerns regarding the autochthonous model used extensively in this work. On the conceptual side, the need for relatively high-dose radiation to activate the compound is somewhat unattractive, as radiation can be associated with short and long-term toxicity, which are often acceptable when radiation is being used as the therapeutic modality, but which seem more difficult to accept when radiation is being used as the activator of the compound rather than as a therapy unto itself.

- What are the noteworthy results?
Overall, this is a comprehensive study of x-ray activated nanoparticle photodynamic therapy for the treatment of bladder cancer. The theory behind x-ray activated photodynamic therapy is explained in Figure 1a/b. The remainder of Figure 1 delineates the specific spectral qualities of the nanoparticle

components. The authors showed the specific in vivo uptake of the nanotransducers into bladder tumor cells in Figure 2, which gives evidence for its use as an imaging modality. Figure 3 and 4 show the specific cytotoxic effects of x-ray activated in vitro in bladder cancer cells. Figure 5 describes the in vivo effects of photodynamic therapy in MNU-induced NMIBC mouse models. Figure 6 and Figure 7 shows the post-operative monitoring capabilities of the nanoparticle technology.

- Will the work be of significance to the field and related fields? How does it compare to the established literature? If the work is not original, please provide relevant references.
Photodynamic therapy is an active area in bladder cancer research. Clinical trials are ongoing to best determine its role in standard treatment, especially of non-muscle invasive disease (NMIBC). Overall, the results of this manuscript provide evidence for the feasibility of coupling a novel technology (i.e. photodynamic therapy) with radiation for the treatment of NMIBC. Detecting recurrence is a challenging clinical paradigm in the treatment of NMIBC and requires frequent invasive cystoscopies and trips to the OR. Regimens which may enhance the sensitivity of cystoscopic evaluation of NMIBC are needed, and this could be one of those regimens.

- Does the work support the conclusions and claims, or is additional evidence needed?
In order to enhance the author's claims of the nanoscintillator technology efficacy in the treatment of NMIBC, further studies may be needed in a more clinically relevant setting. For example, combination therapy with either BCG or other standard-of-care intra-vesical therapy or ADCs could provide the basis for clinical trials alone. Currently, combination treatment with RT alone would not be feasible treatment regimen. In vivo experiments which include a combination with gem/cis and/or immunotherapy could be an appropriate treatment environment (i.e. tri-modal therapy) and efficacy in this setting would be a stronger clinical correlate.

- Are there any flaws in the data analysis, interpretation and conclusions? - Do these prohibit publication or require revision?
Please see detailed comments and requested edits below.

- Is the methodology sound? Does the work meet the expected standards in your field?
The authors chose a carcinogen-induced model of bladder cancer in mice, which is a reasonable and well-established approach. They use this model as a proxy for NMIBC. The authors include both in vitro and in vivo experimental approaches, which are both a standard and necessary to show pre-clinical efficacy. Various relatively simple staining (IHC, imaging, and FACS-based) assays are used to support the author's conclusions, and these are mostly clearly presented in the figures and text.

- Is there enough detail provided in the methods for the work to be reproduced?
While I am not an expert in the development of these x-ray nanoparticles, the rationale behind their use is sound and the protocols for their development appear reproducible. The mouse experiments are certainly feasible and reproducible. The staining assays are also relatively simple and could be easily reproduced.

Specific comments:

Additional description of Rose Bengal (RB) is required

For the MNU mouse model in Fig 2A, how were mice monitored for tumor formation? (ultra-sound? MRI?). When were mice sacrificied relative to MNU treatment start date and/or date of first tumor formation?

It would be worth mentioning if there were any metastasis at any point prior to Day 56 in the mouse experiments (as the lack of metastasis would support its utility as a model of NMIBC).

For experiment summarized in Figure 2F-G, why was NSs-RB-FITC not shown in healthy mice?

For experiments summarized in Figure 3G-J, why was NSs-RB-cRGD + x-ray not tested? Is it because the ROS assay relies on fluorescence readout that would be obscured by FITC-labeled cRGD? If so, this should be stated explicitly, and a ROS assay that does not rely on fluorescence readout should be considered so that the NSs-RB-cRGD compound can be be tested and its impact on ROS generation compared to other compounds (NSs-AEP and NSs-RB) since it seems like the authors believe that NSs-RB-cRGD is the 'lead compound' at this point based on its superior properties.

Additional details regarding the tumor model used for the efficacy studies in Figure 5 are required. How are mice monitored for tumor formation following MNU administration? What is the cause of death in mice that die during the experiment? It is somewhat surprising to me that all mice appear to be randomized at day 70 following MNU administration, and then ~50% are dead within 10 days after randomization. This would suggest that the system is incredibly uniform and predictable in its behavior if all mice have equivalent tumors and are reasonably healthy at 70 days, but then many die within the next 10 days if untreated. Most autochthonous models display significantly more heterogeneity in terms of time to tumor development and survival after developing tumors. Details regarding cause of death (or criteria for sacrifice) are particularly critical when attempting to interpret data from this experiment.

How were x-ray treatments delivered? Were these image-guided treatments or was the entire mouse (or entire pelvis) irradiated? What beam arrangement and RT planning parameters were used?

Do the authors believe that the improved mouse survival observed with NSs-RB-cRGD plus 6 Gy compared to 4 Gy is due to the increased RT dose or increased efficacy of the NSs-RB-cRGD following excitation with 6 vs 4 Gy? It may be difficult to know because a control arm of PBS + 4 Gy was not included.

Presence of absence of "NMIBC signatures" is not a sufficient pathologic assessment of bladders harvested from treated mice. Instead, validated features of NMIBC as determined by H&E and IHC (Ki-67, GATA3, CK5, etc) should be assessed, ideally by a trained pathologist.

The immune cell analyses (Fig. 5e-k) are largely descriptive and do not directly support differences in efficacy among different treatment regimens. Immune infiltration varies widely among bladder tumors and is not clearly related to tumor response in many cases. In my opinion, these immune-based analyses

do not provide strong support for clinically relevant differences in activity among treatment arms.

In Fig 6A, would prefer to label columns with actual treatments rather than roman numerals.

In experiments summarized in Fig 6A-C, it seems like there are opportunities for further informative analyses, such as: (1) what was the average signal intensity at the last scan before the mouse died? This would help establish relationship between signal intensity/properties and clinical disease course. (2) how much tumor was present by pathologic assessment at time of tumor death? This would help establish relationship between signal intensity and pathologic burden of disease.

Reviewer #5 (co-review with Reviewer #4):

I co-reviewed this manuscript with one of the reviewers who provided the listed reports. This is part of the Nature Communications initiative to facilitate training in peer review and to provide appropriate recognition for Early Career Researchers who co-review manuscripts.

Peer Review File

Manuscript title: Full-course NIR-II imaging-navigated fractionated photodynamic therapy of bladder tumours with X-ray-activated nanotransducers

Point-by-point response letter to the reviewers:
We would like to thank all five reviewers and the editor for their constructive suggestions and valuable time, which greatly helped us to improve the quality of our work. We have diligently addressed all the concerns and added new data, evidence, and explanations both in the revised manuscript and the supporting information as highlighted in yellow. We hope the reviewers and the editor are satisfied with the revisions.

Reviewer comments on the initial version:

Reviewer #1 (Remarks to the Author)
He et al report the use of lanthanide nanoparticles activated by X-rays for imaging in NIR-II and photodynamic applications in a murine bladder tumor model.
The manuscript is well written and the work is of interest to the audience of Nat Comm, and should be published after minor recommendations.

Overall response: We appreciate your affirmation of our manuscript that "*The manuscript is well written and the work is of interest to the audience of Nat Comm, and should be published after minor recommendations*".

We fully understand the importance of further characterization of the nanotransducers and have conducted additional experiments with new data and conclusions. More details can be found below.

Comment 1. with ref 22-25 the authors should also add this: Light: Science & Applications (2022) 11:123, doi.org/10.1038/s41377-022-00808-6

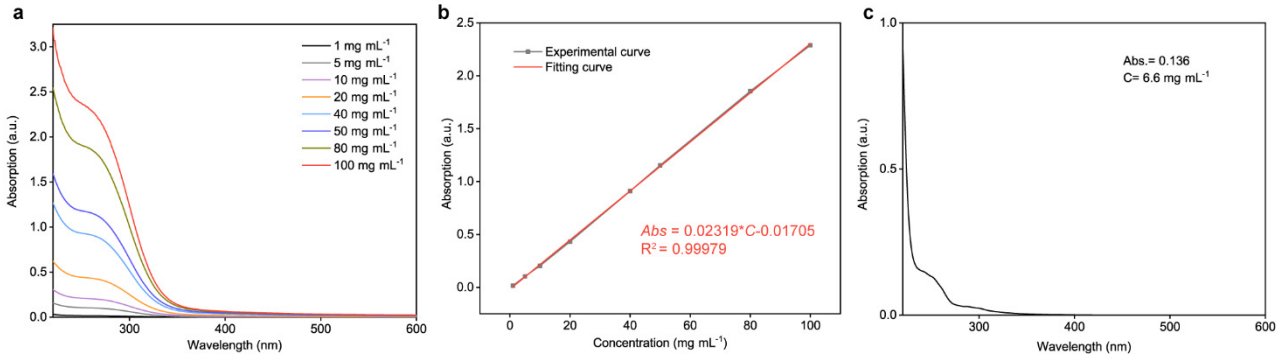
Response: Thank you for your suggestion, the listed literature was found to be of significant supplement to our manuscript and very valuable for broad audiences. It has been cited in the revised manuscript as ref. 26.

Comment 2. do the authors have an idea of the quantity of AEP grafted on the nanoparticles? If not which technique could be used?

Response: We appreciate your valuable suggestion. The quantity of AEP grafted on the nanoparticles can be measured based on the characteristic adsorption peak of AEP at 261 nm. The method is as follows, the absorption spectra at different concentrations were first measured to generate the standard curve of AEP, then all the supernatants after surface modification of AEP on the nanoparticles and washing to remove unconjugated AEP finished were collected to measure the adsorption, thus the quantity of AEP grafted on the

nanoparticles could be calculated.

Particularly, with the feeding amount of NSs to be 100 mg and the amount of AEP to be 750 mg, the concentration of the supernatant was measured to be 6.6 mg·mL^{-1} according to the standard curve with the volume parameter of the supernatant (50 mL). Therefore, the quantity of AEP in the supernatant was 330 mg, thus the mass ratio of AEP onto NSs could be calculated to be (750-330) mg:100 mg = 4.2:1. We have added this detail in the revised manuscript as "*Surface modification of the as-synthesized NSs to convert into hydrophilicity was first conducted by a ligand exchange process using N-Aminoethylpiperazine (AEP) with amino groups for further modification. The mass ratio of AEP onto the NSs was determined to be about 4.2:1 (Supplementary Figure 6)*."



***New* Supplementary Figure 6 | a**, Absorption spectra of AEP at various concentrations. **b**, The linear fitting of AEP absorbance at 261 nm versus concentration. **c**, Absorption spectra of the supernatant of NSs after conjugation with AEP.

Comment 3. do the authors know how this molecule is grafted on the nanoparticles?

Response: We understand your concern about the mechanism of modifying AEP onto the NSs. We do know the mechanism and in fact, the modification processes of AEP were specifically designed based on the higher affinity of the phosphate group of AEP to metal ions of NSs than that of the carboxyl group of the oleic acid ligand (*JACS Au* 2022, 2, 711–722), which is commonly described as a ligand exchange process and has been widely used in literatures, such as *Angew. Chem. Int. Ed. 2013, 52, 6671-6676; Biomaterials 2018, 184, 31-40; Nano Lett. 2022, 22, 8519–8525; Angew. Chem. Int. Ed. 2023, 62, e20231131*.

We have added these details in the revised manuscript as "*Surface modification of the as-synthesized NSs to convert into hydrophilicity was first conducted by a ligand exchange process using N-Aminoethylpiperazine (AEP) with amino groups for further modification.*"

Comments 4: in Fig 2d, the authors show the size of NS measured by DLS after the different coating steps. The size is quite large compared to initial ~25 nm measured by TEM. How do they explain this large increase?

Response: We understand your concern on this issue. The values obtained by TEM and DLS characterizations reflected the dry-state and liquid-state sizes of the NSs, respectively.

Particularly, TEM images depicted the actual size of NSs with a value of ~25 nm, whereas DLS depicted the hydrodynamic diameters of NSs that contain the actual size of NSs with the swollen corona of the surface grafted molecules (150.8, 184.8, and 271.2 nm after different coating steps, respectively). Generally, the sizes measured by DLS were about several times that measured by TEM images (such as *Nat. Photonics* 2019, 13, 525–531, DLS of ~110 nm *versus* TEM of 14.5 nm and *Nat. Commun.* 2023, 14, 1079, DLS of ~112 nm *versus* TEM of 9.8 nm × 13.7 nm).

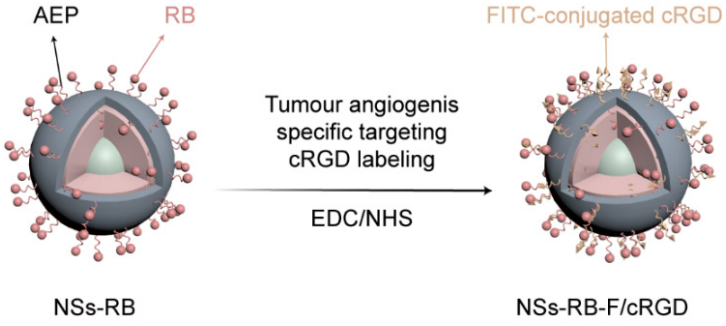
Comment 5: for the grafting of FITC on NS, the authors used EDC/NHS. What is their role?

Response: We appreciate your concern about the synthesis process of NSs-RB-FITC and NSs-RB-cRGD (changed to NSs-RB-F/cRGD in the revised manuscript to highlight all the components) and apologize for the confusion caused by our descriptions. NSs-RB-FITC and NSs-RB-F/cRGD were synthesized separately by grafting commercially purchased FITC-COOH molecules and cRGD-FITC (abbreviated as F/cRGD) peptides onto NSs-RB through the reaction of -COOH groups and -NH_2 groups of unreacted AEP in NSs-RB. The standard method for immobilization of -COOH and -NH_2 groups via covalent amide bond is using the well-known N-ethyl-N′-(3-(dimethylamino)propyl)carbodiimide (EDC) and N-hydroxysuccinimide (NHS) and widely known as EDC/NHS in the field of Chemistry and so on (e.g., *Anal. Biochem.* 1986, 156, 220, *Int. J. Biol. Macromol.* 2020, 161, 550-560). We have revised the expression of NSs-RB-F/cRGD with more synthetic details in the method part of the revised manuscript to make the content clear.

Comment 6: the authors used a FITC-RGD peptide. What is the role of using a FITC peptide if the NS is already labelled?

Response: We appreciate you for this comment and apologize for the confusion caused by our descriptions. As we have described in response to comment 5 that the target NSs-RB-F/cRGD and homologous NSs-RB-FITC were separately synthesized from NSs-RB by grafting commercially purchased F/cRGD peptides and FITC-COOH molecules through EDC/NHS, other than synthesizing NSs-RB-F/cRGD from NSs-RB-FITC.

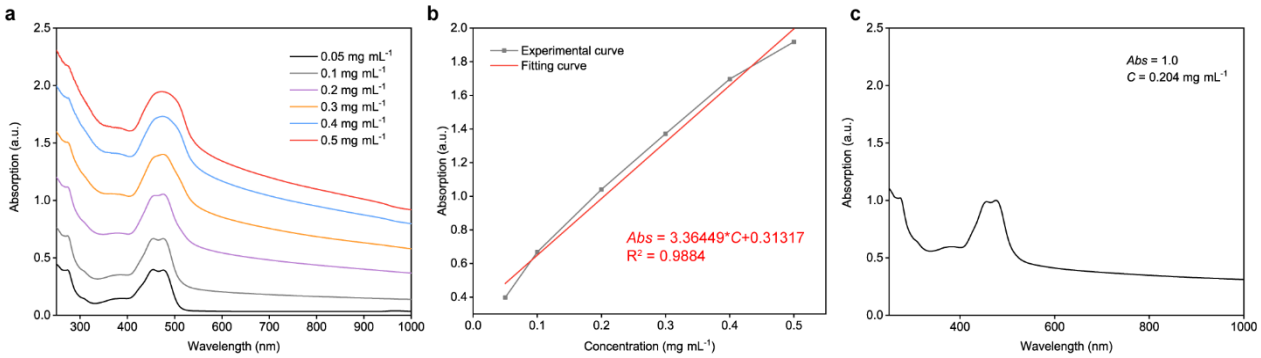
To make the content clear, we have revised the expression of “NSs-RB-cRGD” into "NSs-RB-F/cRGD" in the revised **Figure 2c** and all other related figures throughout the manuscript.



***Revised* Figure 2 | c**, Surface functionalization of nanotransducers by cRGD-FITC (F/cRGD) peptides.

Comment 7: do the authors have an idea of the amount of peptide grafted on the NS? If not which technique could be used to determine this amount?

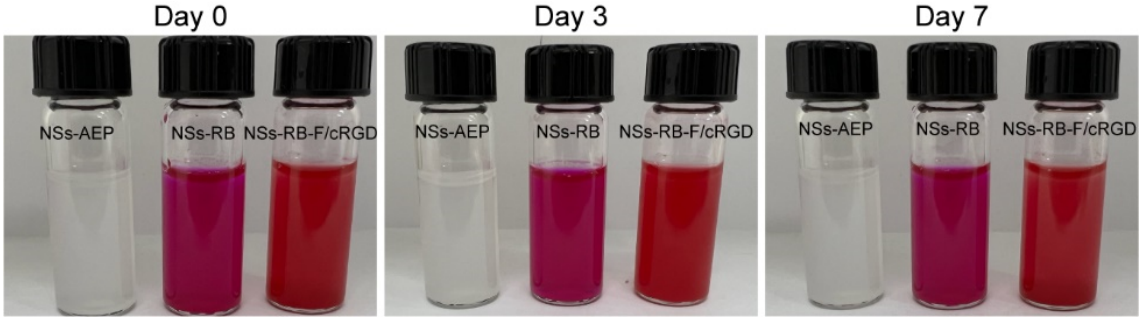
Response: We appreciate your valuable suggestion, and we can determine the amount of peptide grafted on the NS. Particularly, the strategy is like that of comment 2 to determine the quantity of AEP grafted on the nanoparticles because cRGD-FITC peptides (F/cRGD) also possess a characteristic absorbance peak at 476 nm. Therefore, by establishing the standard curve of F/cRGD peptides and measuring the absorbance value of the supernatant after the conjugation and wash procedures, the feeding mass ratio could be calculated. Particularly, with the feeding mass amounts of NSs-RB and cRGD of 530 mg and 10 mg and the volume of supernatant to be 10 mL, the mass ratio of F/cRGD peptides onto the NS was determined to be 7.96:530 with the equation of (10-10*0.204):530. We have also added these details in the revised manuscript as "*The mass ratio of F/cRGD peptides onto NSs-RB was estimated to 7.96:530 (Supplementary Figure 9).*"



***New* Supplementary Figure 9 | a**, Absorption spectra of F/cRGD peptides at various concentrations. **b**, The linear fitting of F/cRGD peptides absorbance peak at 476 nm versus concentration. **c**, Absorption spectra of the supernatant after conjugation with F/cRGD peptides.

Comment 8: are the nanoparticles stable in injection medium?

Response: Thank you for your suggestion. We have conducted the stability investigations of the nanoparticles in the injection medium of PBS (pH 7.4) and observed that all the NSs-AEP, NSs-RB, and NSs-RB-F/cRGD were found with excellent stability over 7 days, which were sufficient for the in vitro and in vivo experiments.



***New* Supplementary Figure 12 |** Stability of NSs-AEP, NSs-RB, and NSs-RB-F/cRGD dispersed in PBS at different times.

Comment 9: how many nanoparticles are injected?

Response: Thank you for your valuable comment. The amounts of nanoparticles including NSs-AEP, NSs-RB, and NSs-RB-F/cRGD that were intravesically instilled into the bladder were all 10 mg mL^{-1} (standardized on the mass of $NaGdF_4$:Ce,Tb@$NaGdF_4$:Nd@$NaLuF_4$ nanoparticles) and 100 μL. The injection dose was calculated to be 1.0 mg per mouse, which was similar or less than that widely used in bladder tumour-bearing mouse models (*Sci. Adv.* 2023, 9, eabq8225; *Chem* 2020, 6, 2283–2299) or other types of tumour mouse models (*Nano Lett.* 2019, 19, 10, 6772–6780; *Adv. Funct. Mater.* 2020, 30, 2001166).

Reviewer #2 (Remarks to the Author):
The authors developed non-invasive fractionated photodynamic therapy (f-PDT) of bladder cancer with full-course real-time NIR-II imaging based on engineered X-ray-activated nanotransducers that contain lanthanide-doped nanoscintillators with concurrent emissions in visible and the second near-infrared (NIR-II) regions and conjugated photosensitizers. This is an interesting study, but there are several issues needed to addressed before further consideration.

Overall response: We appreciate your affirmation of our manuscript, especially "*This is an interesting study*", and the recommendation to be further considered for publication.

We truly thank you for all critical comments on materials design, targeted ability, and in vivo experiments, and have conducted additional experiments as suggested. The supplemental data were in good consistency with our previous results and conclusions and addressed the mentioned issues. More details can be found below.

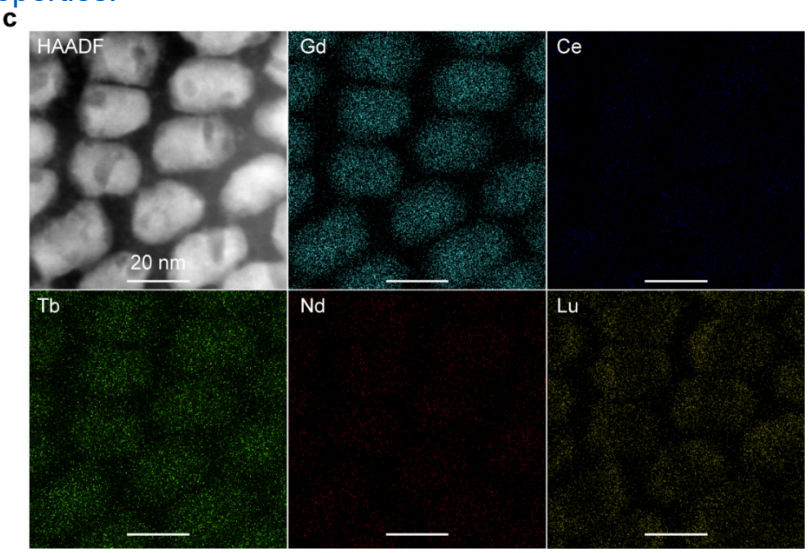
Comment 1: The authors claim that the hexagonal Ln-NSs exhibit more intense X-ray-activated green and NIR-II radioluminescence than the rod-shaped Ln-NSs with anisotropic epitaxial growth. Why would this happen? The mechanism of this phenomenon need to be further explained.

Response: We thank you for this valuable suggestion and understand your concern. We have revised the content with more mechanism descriptions and extra data.

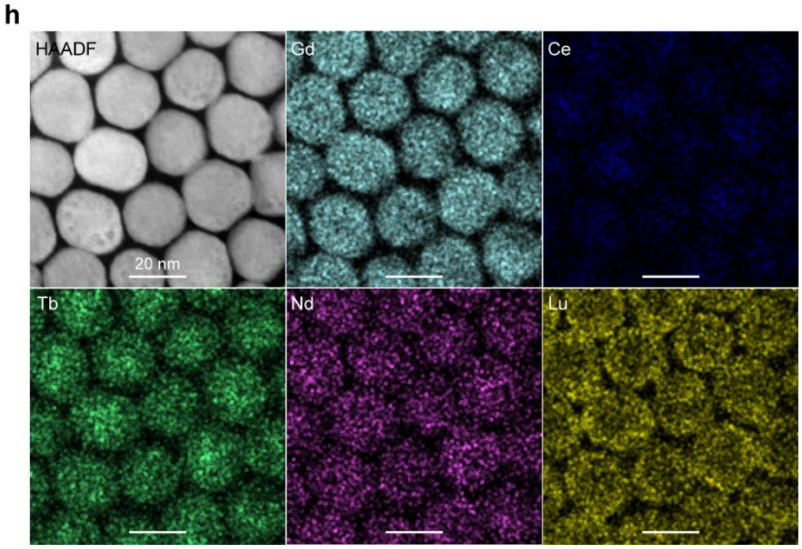
Briefly, in the previous manuscript, we first engineered both the hexagonal and rod-like Ln-NSs and observed the phenomenon that hexagonal Ln-NSs exhibited more intense X-ray-activated luminescence than that of rod-like Ln-NSs (**Supplementary Figures 2** and **3**). A similar phenomenon has also been revealed in literatures (ref. 27,28) and explained to be

contributed by the better passivation effect of isotropic epitaxial growth in hexagonal Ln-NSs to diminish nonradiative relaxation and surface quenching effect.

In support of this mechanism, we conducted energy dispersive spectroscopy (EDS) and indeed found that the rod-like Ln-NSs with anisotropic epitaxial growth had an uneven distribution of Nd out layer and the defective shell growth (**Supplementary Figure 2c**), while the hexagonal Ln-NSs with isotropic epitaxial growth has a homogeneous distribution of Nd or Lu elements (**Supplementary Figure 1h**). Therefore, EDS results supported the mechanism of better passivation effect by isotropic epitaxial growth in hexagonal Ln-NSs to reduce non-radiative relaxation and surface quenching in yielding better X-ray-activated luminescence properties.

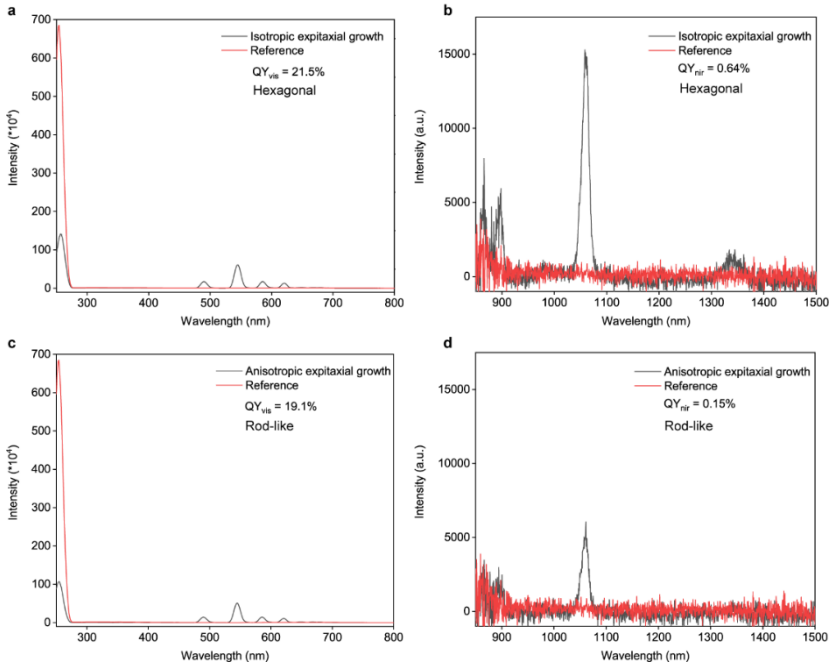


Supplementary Figure 2 | c, High-angle annular dark-field (HAADF) and energy dispersive spectroscopy (EDS) of rod-like $NaGdF_4$:Ce,Tb@$NaGdF_4$:Nd@$NaLuF_4$. The color symbol of each element has been revised to be the same as that shown in Supplementary Figure 3.



Supplementary Figure 1 | h, HAADF and EDS of hexagonal $NaGdF_4$:Ce,Tb@$NaGdF_4$:Nd@$NaLuF_4$. The color symbol of each element has been revised to be the same as that shown in Supplementary Figure 2.

As inspired by reviewer 2, to further support the mechanism and illustrate the differences in luminescence properties between these two types of epitaxial growth, we have conducted additional tests on the absolute fluorescence quantum efficiency. It could be found that both the values of X-ray-activated green and NIR-II luminescence of the hexagonal Ln-NSs were measured to be higher than that of rod-like Ln-NSs (21.5% *versus* 19.1% and 0.64% *versus* 0.15%) (**Supplementary Figure 4**). Being one of the most important parameters in characterizing the intrinsic properties of luminescent materials (*Nat. Protoc. 2013, 8, 1535–1550*), the absolute fluorescence quantum yields further strengthened our conclusion.



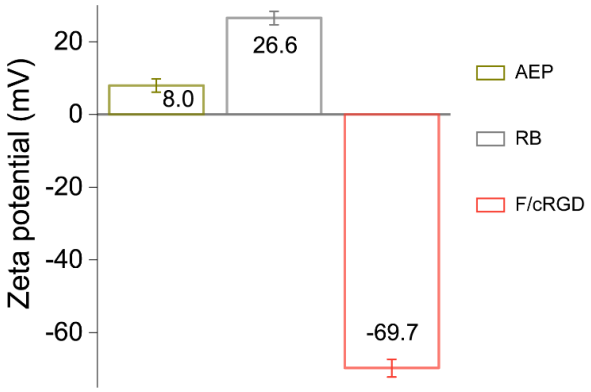
***New* Supplementary Figure 4 | a,b** Absolute fluorescence quantum yield of hexagonal $NaGdF_4$:Ce,Tb@$NaGdF_4$:Nd@$NaLuF_4$ with isotropic epitaxial growth in visible (**a**) and NIR-II spectra (**b**). **c,d** Absolute fluorescence quantum yield of rod-like $NaGdF_4$:Ce,Tb@$NaGdF_4$:Nd@$NaLuF_4$ with anisotropic epitaxial growth in visible (**c**) and NIR-II spectra (**d**).

We have added these additional data in the revised manuscript as "*The more intense X-ray-activated green and NIR-II luminescence of hexagonal Ln-Ns with isotropic epitaxial growth were further confirmed by the absolute fluorescence quantum efficiency estimation (Supplementary Figure 4). Together with the EDS results (Supplementary Figure 1h and 2c), it can be inferred that this phenomenon was attributed to the better passivation effect of isotropic epitaxial growth of hexagonal Ln-Ns*[27,28]*…*"

Comment 2: What is the reason for the change in Zeta potential from +8.9 eV for NSs-AEP and +21.5 eV for NSs-RB to -40.3 eV for NSs-RB-cRGD? Is it the reason for the introduction of cRGD? Authors should explain it in detail.

Response: We thank you for this valuable suggestion. To provide evidence of the changes in the Zeta potential of different nanoformulations, we have estimated the Zeta potentials of AEP, RB, and cRGD-FITC (F/cRGD) and the values were measured to be +8.0, +26.6, and

-69.7 eV (**Supplementary Figure 11**), respectively. Therefore, it could be inferred that after surface ligand exchange of as-synthesized NSs, the yield NSs-AEP showed a positive value of +8.9 eV due to the presence of AEP, and the values of NSs-RB after conjugation of RB and NSs-RB-F/cRGD after conjugation of F/cRGD peptides were correspondingly changed to +21.5 and -40.3 eV, respectively.



***New* Supplementary Figure 11 |** Zeta potentials of AEP, RB, and F/cRGD peptides.

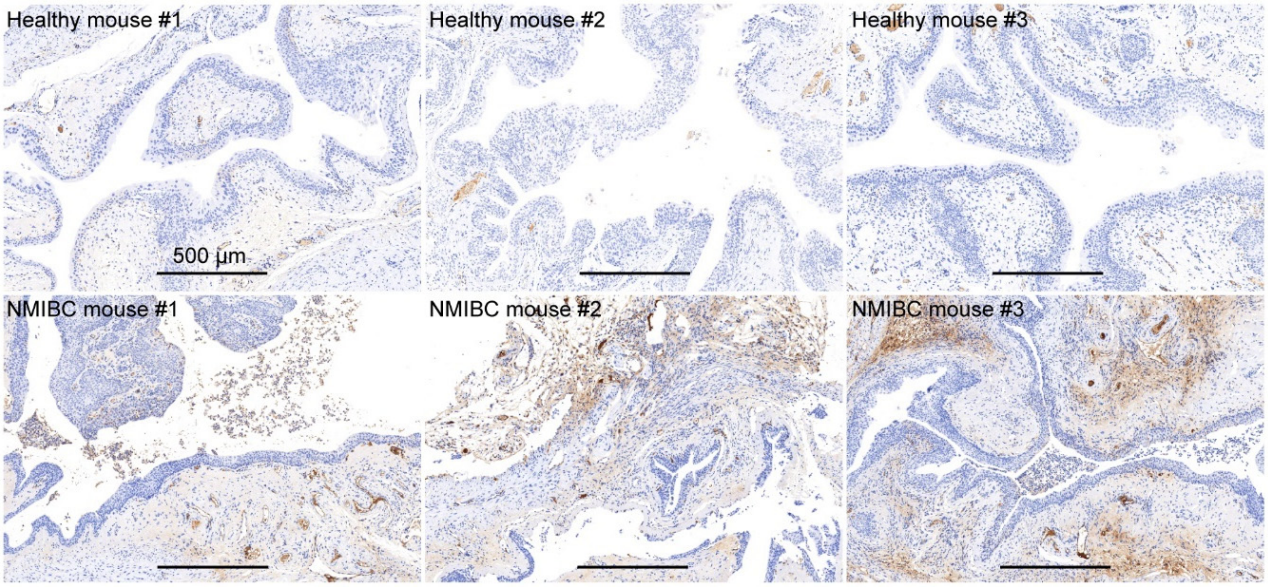
We have also added the values of Zeta potentials of AEP, RB, and F/cRGD in the revised manuscript as **Supplementary Figure 11** with descriptions as "*Meanwhile, Zeta potentials varied from +8.9 eV of NSs-AEP and +21.5 eV of NSs-RB to -40.3 eV of NSs-RB-F/cRGD after conjugation of AEP, RB, and F/cRGD* ***(****Figure 2e, Supplementary Figure 11 and 12)…"*

Comment 3: The authors used infused imaging to verify the targeting of NSs-RB-cRGD, but there are certain problems in the current study. First, the authors did not verify the expression of $\alpha_v\beta_3$ in tumors and normal tissues in the induction model. Second, imaging validations of different tumor cell lines with high and low $\alpha_v\beta_3$ expression are also necessary to demonstrate the targeted uptake ability of NSs-RB-cRGD. Third, as can be seen in Figure 2b, the induced tumor lesions are diffusely distributed, while in the fluorescence images in Figure 2f, the fluorescence distribution is a single bright spot. The fluorescence pattern of the non-diffuse distribution may be caused by infused residue or non-specific adsorption. It is recommended that the authors supplement more relevant and solid results to prove the specificity.

Response: We appreciate these valuable comments and have supplemented more relevant and solid results to further prove and strengthen the specificity as suggested.

Firstly, in terms of $\alpha_v\beta_3$ expression in tumours and normal tissues in the induction model, we conducted immunohistochemistry (IHC) analysis (Abcam, Anti-Integrin alpha V beta 3 [BV3], ab7166) on bladder tissues of three NMIBC and three healthy mice (Oncogenesis 2020, 9, 69), respectively. As revealed in **Supplementary Figure 10**, the $\alpha_v\beta_3$ integrin expression was observed to be highly expressed in the NMIBC bladders with low levels in the normal sections, and rather low levels were observed in the bladders of healthy mice. The verified $\alpha_v\beta_3$ expression in tumours and normal tissues could further support the tumour-targeting capability of the NSs-RB-F/cRGD. This was also the reason that cRGD-based

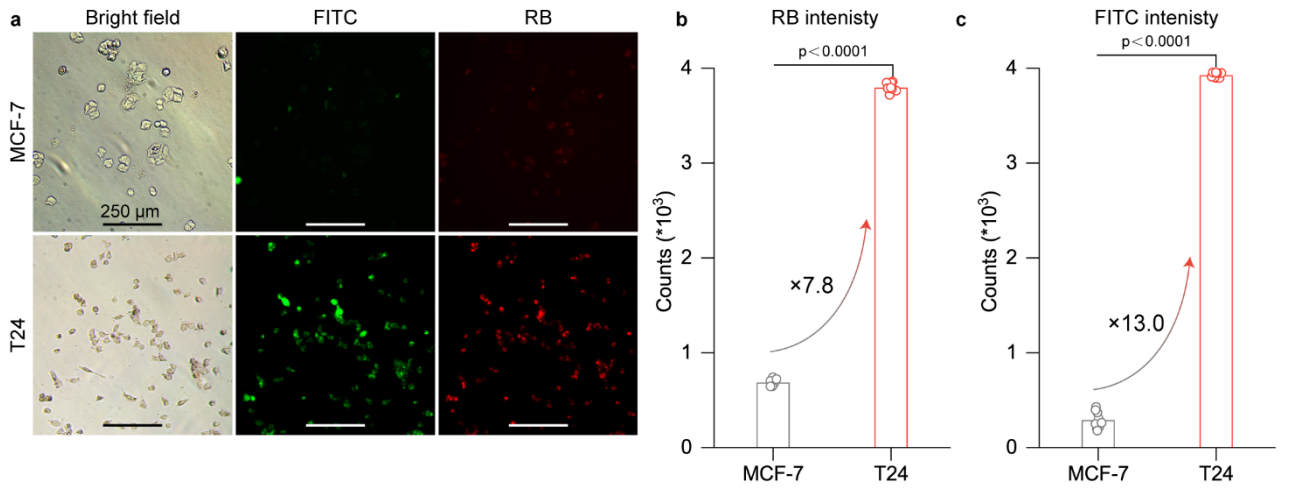
nanotechnology has been widely used as a promising approach to deliver anticancer nanoagents (*Nat. Mater.* 2023, 22, 1421–1429; *Nat. Commun.* 2021, 12, 2174; *Angew. Chem. Int. Ed.* 2021, 60, 8938-8947).



***New* Supplementary Figure 10 |** Expression of $\alpha_v\beta_3$ integrin in bladder tissues of NMIBC or healthy mice (Brown: $\alpha_v\beta_3$ Integrin-expressing cells; blue: nucleus).

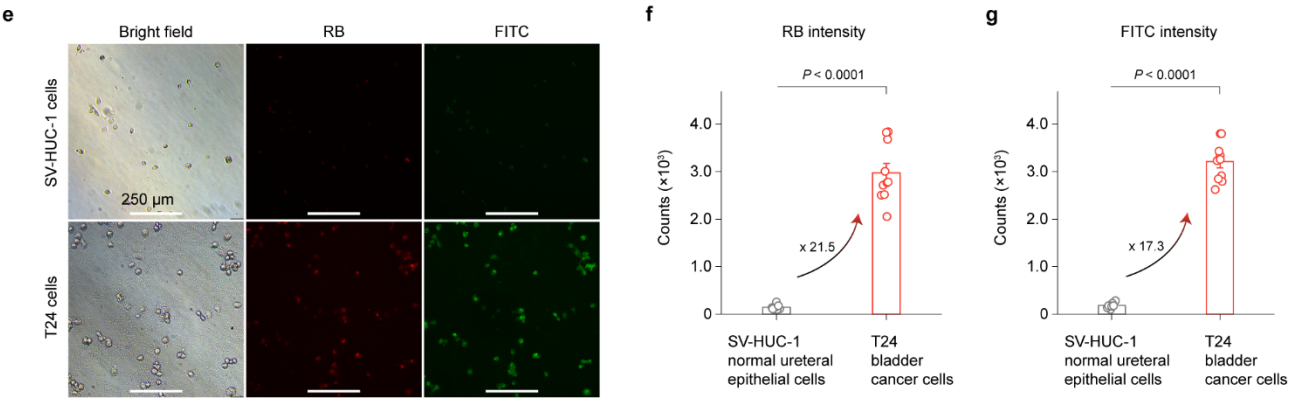
Secondly, to demonstrate the targeted uptake ability of NSs-RB-F/cRGD through imaging validations of different tumour cell lines with high and low $\alpha_v\beta_3$ expression as suggested, we adopted the typical cell lines of breast cancer cells of MCF-7 with low $\alpha_v\beta_3$ integrin expression (*Biomaterials* 2014, 35, 6106-6117) and the bladder cancer cells of T24 with high $\alpha_v\beta_3$ integrin expression (*Biomaterials* 2021, 264, 120434) and estimated their uptake efficiency. As shown in **Supplementary Figure 16**, T24 cells were found with much more intense RB and FITC signals with values to be about 7.8 and 13.0-fold higher than that observed in MCF-7 cells, demonstrating that the amounts of $\alpha_v\beta_3$ integrin expression would affect the targeted uptake ability of NSs-RB-F/cRGD. These new data and evidence further supported our conclusion on improved targeted uptake ability of NSs-RB-F/cRGD.

We have added these new details in the revised manuscript "*Moreover, the RB and FITC intensities detected in breast cancer cells of MCF-7 with low $\alpha_v\beta_3$ integrin expression were much lower than those in bladder cancer cells of T24 with high $\alpha_v\beta_3$ integrin expression (Supplementary Figure 16), indicating the high affinity of F/*cRGD *peptide-modified nanotransducers to overexpressed $\alpha_v\beta_3$ in NMIBC.*"



***New* Supplementary Figure 16 | a,b,c**, Fluorescence imaging (**a**) and quantitative RB (**b**) and FITC fluorescence intensities (**c**) in breast cancer cells of MCF-7 and bladder cancer cells of T24 incubated with NSs-RB-F/cRGD (50 μg mL^{-1}).

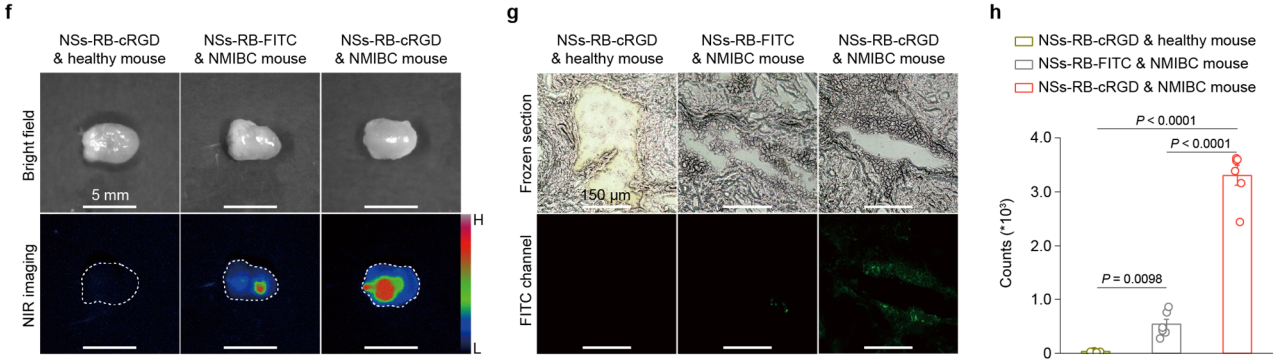
Notably, the relationship between the targeted uptake ability of NSs-RB-F/cRGD and $\alpha_v\beta_3$ integrin expression could also be deduced by the diverse uptake ability of NSs-RB-F/cRGD between the normal human urinary tract epithelial cells of SV-HUC-1 with low $\alpha_v\beta_3$ integrin expression and the T24 cells with high $\alpha_v\beta_3$ integrin expression that showed in the previous work. Briefly, the uptake amount of NSs-RB-F/cRGD by T24 cells was found to be about 20 times higher than that of SV-HUC-1 cells from both FITC and RB channels (**Supplementary Figure 14e-g**).



Supplementary Figure 14 | e,f,g, Fluorescence imaging (**e**) and quantitative RB (**f**) and FITC fluorescence intensities (**g**) in normal ureteral epithelial cells of SV-HUC-1 and bladder cancer cells of T24 incubated with NSs-RB-F/cRGD (50 μg mL^{-1}).

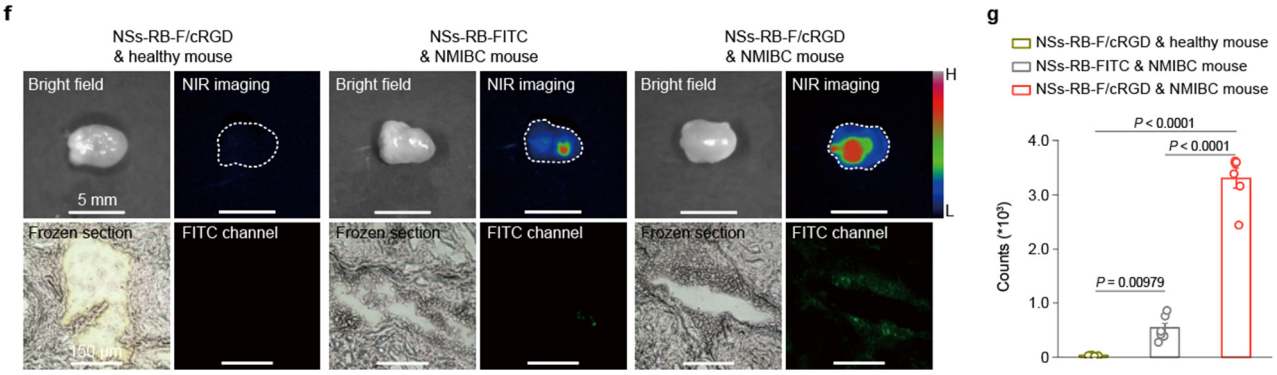
Thirdly, in terms of the tumour specificity issue with diffusely distributed tumour lesions in **Figure 2b** and a single bright spot of fluorescence distribution in the original version of **Figure 2f**, we apologize for the confusion caused by our concise expression. **Figure 2b** was taken with the inner surface of bladder tissues exposed initially to show the tumour lesions and successful establishment of NMIBC with no intravesical instillation of NSs-RB-F/cRGD. The original version of **Figure 2f** was taken from the original outer surface of bladder tissues that were intravesically instilled with NSs-RB-FITC or NSs-RB-F/cRGD but not with the inner

surface exposed to avoid detachment of tumour lesions considering that they were further employed to perform fluorescence imaging with frozen slices (the original version of **Figure 2g** & **Supplementary Figure 8d-g**).



***The original version of* Figure 2 | f**, Ex vivo NIR-II fluorescence imaging (ex: 808 nm) of bladders dissected from the NSs-RB-F/cRGD-treated healthy mouse and the NSs-RB-FITC-treated and NSs-RB-F/cRGD-treated NMIBC mice. **g**, Fluorescence imaging of corresponding frozen slices (FITC channel, ex/em: 460-500/512-542 nm) of bladders dissected from the NSs-RB-F/cRGD-treated healthy mouse and the NSs-RB-FITC-treated and NSs-RB-F/cRGD-treated NMIBC mice. **h**, Quantitative FITC fluorescence signals with statistical analysis in **g**.

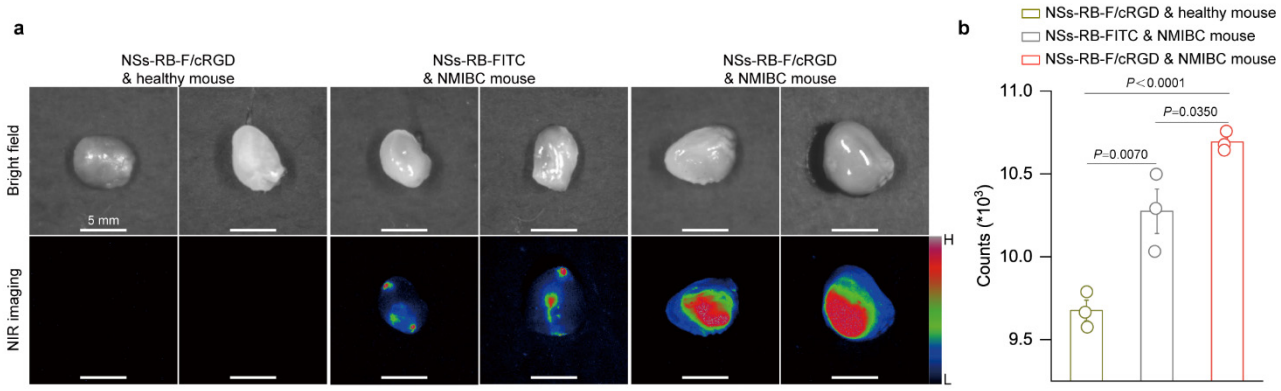
To eliminate possible confusion or misunderstanding, we have emphasized the different states of tumour tissues in **Figure 2b** from "bladders externalized dissected" to "bladders externalized dissected (inner surface exposed)" in the revised manuscript. Meanwhile, to logically present the relationship between the bladder tissues and the corresponding frozen slices, we have also reorganized the original version of **Figure 2f** and the original version of **Figure 2g,h** into a new version of **Figure 2f,g** in the revised manuscript.



***The revised new version of* Figure 2 | f**, Ex vivo NIR-II fluorescence imaging (ex: 808 nm) of bladders and the corresponding frozen slices (FITC channel, ex/em: 460-500/512-542 nm) that dissected from the NSs-RB-F/cRGD-treated healthy mouse and the NSs-RB-FITC-treated and NSs-RB-F/cRGD-treated NMIBC mice. **g**, Quantitative FITC fluorescence signals with statistical analysis on the corresponding frozen slices in **f**.

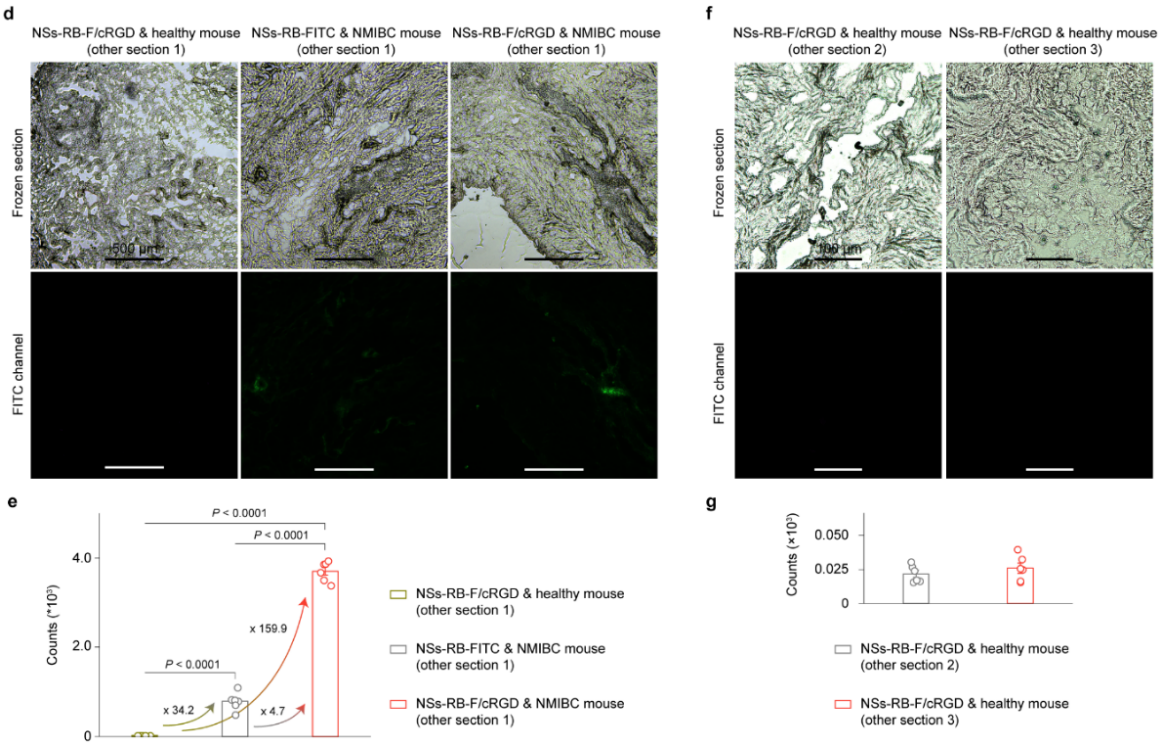
The reasons that the fluorescence distribution of bladder tissues was a single bright spot in **Figure 2f** were mainly as follows: (1) the urothelial carcinoma of the bladder is a typical

multifocal papillary tumour as showed in **Figure 2b**, the different sizes of papillary tumours might lead to different accumulation amount of NSs-RB-F/cRGD with different NIR-II luminescence intensity in different parts of the tumour tissues as could be found in **Figure 2f**; (2) fluorescence imaging is commonly known to suffer from tissue scattering (*Nat. Biomed. Eng.* 2020, 4, 259–271; *Lancet Oncol.* 2019, 20, e354–67). Therefore, when bladder tissues are in their original state, one can image that the tumour lesions would condense and overlap, thus leading to the appearance of **Figure 2f** with "a single bright spot" as also shown in most in vivo or ex vivo fluorescence images. We also provided the parallel ex vivo NIR-II fluorescence imaging of the frozen bladders from NMIBC mice in **Supplementary Figure 13**. It could be found that the fluorescence distribution was also like a single large bright spot, which was in good consistency with that in the original version of **Figure 2f**, demonstrating the reproducibility of our protocol and tumour targeting capability of NSs-RB-F/cRGD.



***New* Supplementary Figure 13 | a**, Ex vivo NIR-II fluorescence imaging (ex: 808 nm) of bladders dissected from the NSs-RB-F/cRGD-treated healthy mice and the NSs-RB-FITC-treated and NSs-RB-F/cRGD-treated NMIBC mice. **b**, Quantitative NIR-II fluorescence signals with statistical analysis in **a**. Data in **b** were shown as mean ± s.e.m. The *P* values in **b** were calculated by one-way ANOVA and Tukey multiple-comparison test.

Moreover, we have to say that the fluorescence pattern of the non-diffuse distribution was entirely not related to any infused residue or non-specific adsorption because all the healthy and NMIBC mice were intravesically instilled with PBS to wash out unaccumulated nanoparticles following 1 h after intravesical instillation of NSs-RB-FITC or NSs-RB-F/cRGD before conducting NIR-II fluorescence imaging and f-PDT. We can see from the revised version of **Figure 2f,g** and **Supplementary Figure 8d-g** that the corresponding frozen sections of bladders from NSs-RB-F/cRGD-treated healthy mice were extremely low NIR-II fluorescence signals of the frozen slices, while that from NSs-RB-FITC-treated bladder mice exhibited about 20 times stronger signals and that from NSs-RB-F/cRGD-treated bladder mice with more than 100 times stronger signals, indicating no apparent infused residue or non-specific adsorption in the bladders in contributing the tumour-targeting capability.



Supplementary Figure 8 | d,**e**, Fluorescence imaging of frozen slices (FITC channel, ex/em: 460-500/512-542 nm) (**d**) and quantitative FITC fluorescence signals with statistical analysis (**e**) of dissected bladders from a healthy mouse infused with NSs-RB-F/cRGD and NMIBC mice infused with NSs-RB-FITC and NSs-RB-F/cRGD. **f**,**g**, Fluorescence imaging of frozen slices (FITC channel, ex/em: 460-500/512-542 nm) (**f**) and quantitative FITC fluorescence signals (**g**) in other two sections of the dissected bladder from the healthy mouse infused with NSs-RB-F/cRGD as control.

We have also provided the above new data and explanations in the revised manuscript to make the content more robust and understandable as "…*Notably, the difference between the bright spots in Figure 2f and Supplementary Figure 13 and the diffusely distributed tumour lesions in Figure 2b was mainly because they were taken from different angles of view of bladders and the overlapping of tumour lesions when inside bladder tissue and also the tissue scattering of NIR-II fluorescence.*"

Comment 4: The authors proposed that nanoscintillators play an important role in the generation of cytotoxic hydroxyl radicals (·OH), whether there is further theoretical support and data validation?

Response: We thank you for this valuable suggestion. There was theoretical support and data validation in the previous manuscript to support the generation of cytotoxic hydroxyl radicals (·OH). It was described and demonstrated as the radiosensitization effect because this term has been academically used both in radiological medicine and nanomedicine to describe the capability of nanomaterials to destroy tumour cells or tissues by producing free radicals (mainly ·OH) under irradiation of X-rays (*Chem. Soc. Rev.* 2019, 48, 540-557, and

ref 45,46). High-atomic-number elements, such as the Gd, Ce, Tb, Nd, and Lu, intrinsically have strong radiosensitization effects in generating ·OH under radiation (ref. 45,46).

Briefly, among all the cytotoxicity estimation (**Figure 3b**, **Supplementary Figure 17c** & **Figure 4a-d**) and ROS estimation (**Figure 3g-j**), the cytotoxicity of cells treated with NSs-AEP+X-ray was attributed to the radiosensitization effect of the nanoscintillators and all the data could indicate the existence of ·OH. To rigorously assess the radiosensitization effect, we also conducted the most recommended clonogenic survival assays and DNA damage assays (*Nat. Protoc.* 2016, 1, 2315–2319, *Mol. Cancer* 2019, 18, 71, *Nat. Commun.* 2017, 8, 14432, and *Nat. Rev. Cancer* 2023, 23, 78–94). As shown in **Figure 3e,f** & **Figure 3d**, NSs-AEP+X-ray could greatly destroy tumour cells with decreasing survival fractions along with the increase in X-rays and induced obvious γ-H2AX signals in cell nuclei compared to X-ray. All the results could demonstrate the capability of radiosensitization of NSs, namely the generation of ·OH. Notably, the radiosensitization effect with ·OH generation was also the dominating reason that the combination of NSs-AEP+6 Gy exhibited better efficiency in inhibiting tumour growth of autochthonous bladder tumours than pure 6 Gy X-ray irradiation (**Figure 5a-c**). On this basis, NSs-RB+X-ray and NSs-RB-F/cRGD generated numerous ·OH with $^1O_2$ by the activation of RB, thus enabling more robust cytotoxicity and tumour inhibition effects than NSs-AEP+X-ray both in vitro and in vivo.

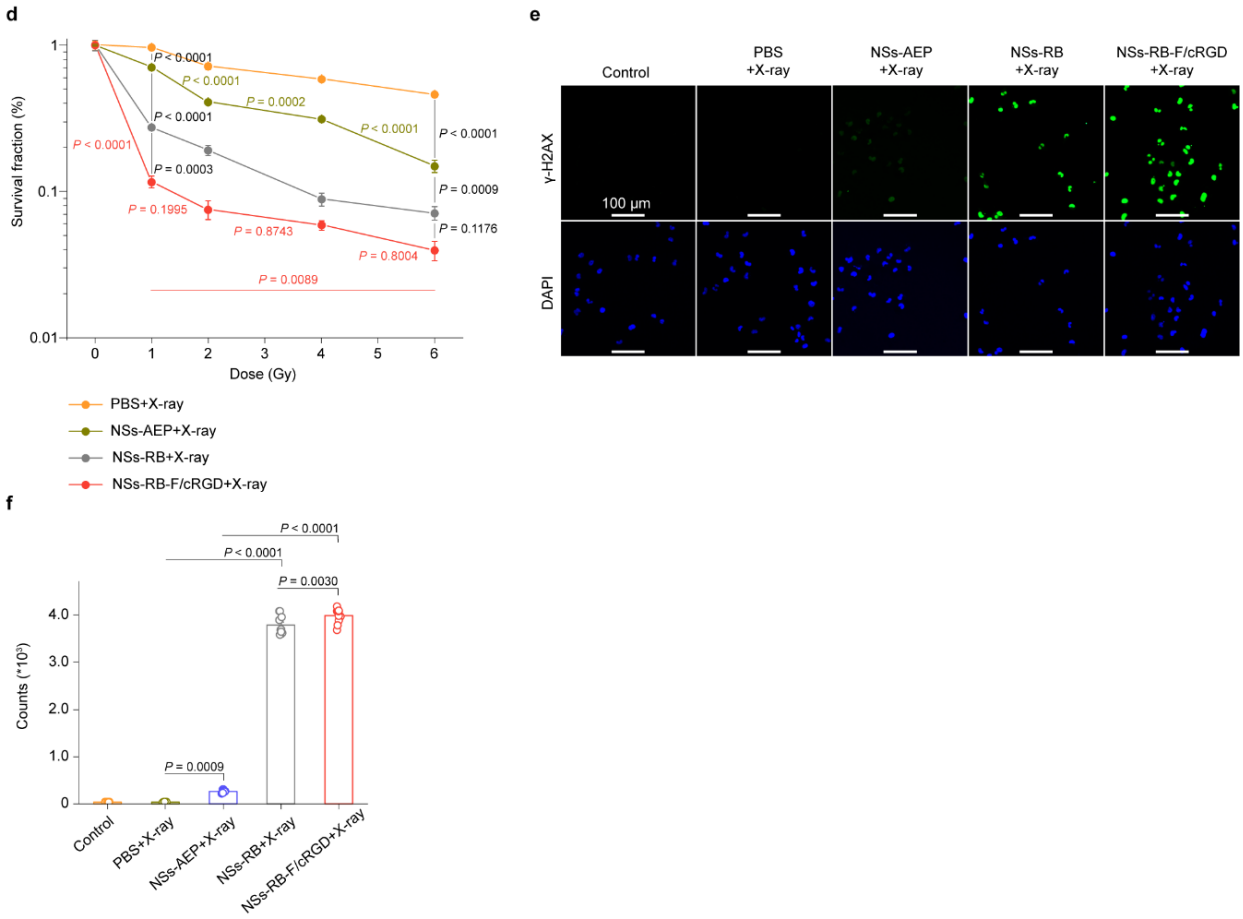


Figure 3 | d, Survival fractions of T24 cells incubated with NSs-AEP, NSs-RB, and NSs-RB-F/cRGD under various X-ray doses (50 μg mL^{-1}). **e**,**f**, Fluorescence images (**e**) and signal

quantification (**f**) of γ-H2AX immunofluorescence analysis of T24 cells treated with NSs-AEP, NSs-RB, and NSs-RB-F/cRGD (50 μg mL^{-1}) under 1-Gy radiation. Data in **d** and **f** were shown as mean ± s.e.m. The *P* values in **d** and **f** were calculated by one-way ANOVA and Tukey multiple-comparison test.

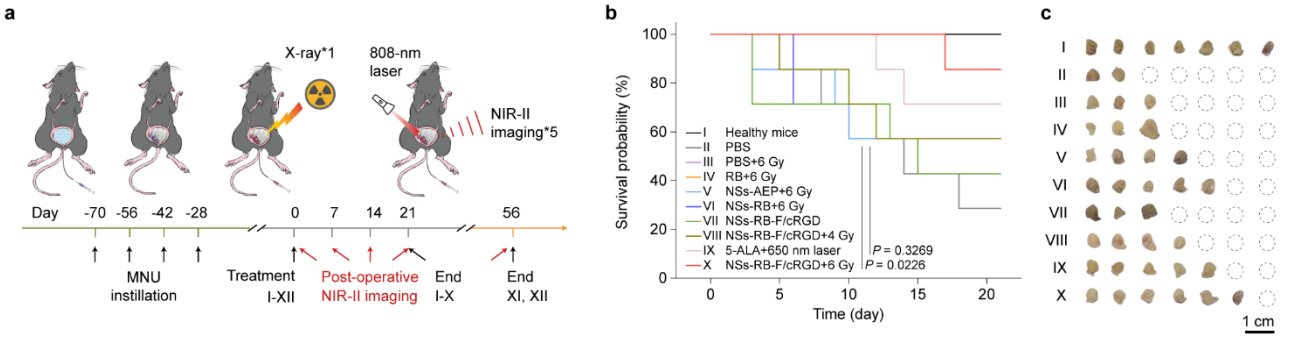
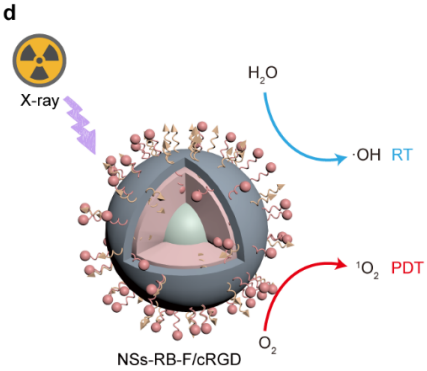


Figure 5 | Tumour regression by non-invasive single-f-PDT. a, Schematic illustration of the experimental protocols for single-f-PDT. **b**, Survival probability of NMIBC mice receiving different treatments for 21 days. **c**, Photographs of bladders dissected from survived mice at day 21.

To make the content more understandable, we have also provided a scheme to illustrate this intrinsic radiosensitization feature of the nanoscintillators (**Supplementary Figure 17d**) in the revised manuscript.



***New* Supplementary Figure 17 | d**, Mechanism of radiotherapy and photodynamic therapy based on NSs-RB-F/cRGD.

Comment 5: Does tumor necrosis induced by radiotherapy/photodynamic therapy affect tumor uptake of the probe and thus the fluorescence signal? If so, does this introduce additional errors in the therapeutic effect evaluation given by the NIR-II fluorescence imaging?

Response: We understand your concern and appreciate your insightful thinking. However, we inferred that the tumour necrosis should not introduce additional errors due to the following two main reasons:

Firstly, unlike solid tumours or tumours in other organs, necrotic bladder tumour cells are rapidly cleared out from the body through urine (*Clin. Transl. Disc.* 2023, 3, e183), therefore, urinary exfoliated tumour cell is widely used in the diagnosis of bladder cancer in the clinic

(*Nat. Rev. Urol.* 2023, 20, 597–614; *Br. J. Cancer* 2014, 130, 369–379). Besides, in our work to perform NIR-II fluorescence imaging at each time point, we perfused with PBS to wash out untargeted nanotransducers after intravesically instilled NSs-RB-F/cRGD into bladders for 1 h. We observed no obvious necrotic tumour cells in H&E staining of tumour slices throughout the project (Group II-X in **Figure 5d**; Group XI-XII in **Figure 6e**; G1&G2 in **Figure 7h**). Under this circumstance, we believe that little tumour necrosis would be firmly attached in NMIBC to accumulated nanotransducers to perform NIR-II fluorescence imaging.

Secondly, tumour accumulation of NSs-RB-F/cRGD after intravesical instillation into the bladder was mainly dependent on the affinity to integrin $\alpha_v\beta_3$ and $\alpha_v\beta_3$ was reported to be highly expressed on the surface of tumour neovascular endothelial cells and living tumour cells. However, tumour necrosis is a common pathway during radiotherapy/photodynamic therapy and a histopathological term that describes tissue death in cancers (*Nat. Commun.* 2020, 11, 5424). Previous literatures have reported that tumour necrosis factors would attenuate neovascularization in tumours (*Eur. Heart J.* 2023, 44, ehad655.325) and ionizing radiation could lead to vascular damage (*Commun. Biol.* 2023, 6, 571). It has also been reported that even with excellent targeting capability to the highly metastatic 4T1 mammary tumours, little amount of fluorescence molecules would accumulate in the necrotic core of tumours (*Mol. Pharmaceutics* 2014, 11, 2896–2905). Therefore, we envisaged that no accumulation of NSs-RB-F/cRGD with additional errors in NIR-II fluorescence imaging would happen even if some tumour necrosis existed in the multifocal papillary urothelial carcinoma of the bladder.

We thank you for this insightful comment on the relationship between tumour necrosis and fluorescence imaging, as literatures have reported the use of targeted fluorescence imaging to guide cancer treatment (*Adv. Mater.* 2022, 34, e2201042; *Chem* 2020, 6, 2283–2299) but seldom focused on this issue. Considering the MNU-induced bladder tumour mice model adopted in our work was not suitable for further investigation, we have included this issue in the discussion part of the revised manuscript as "*Third, to establish more precise and accurate non-invasive imaging modality, the relationship between tumour necrosis or necrotic tissue and fluorescence signals after treatment would also be further investigated by using large animal models or tissues.*"

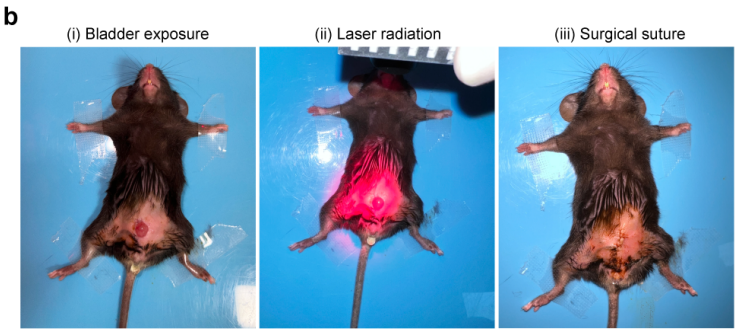
Comment 6: The authors claim that the whole process of non-invasive real-time NIR-II imaging and on-demand use of f-PDT are reliable. However, the treatment effect of this method is not compared with the traditional invasive treatment effect. The superiority of the proposed treatment effect should be further verified.

Response: We appreciate your insightful suggestion on this issue and understand your concern, as we can see from the comment that you take much account of the reliability and robustness of the whole process of non-invasive real-time NIR-II imaging and on-demand f-PDT as we did. The reasons that we did/could not conduct traditional invasive treatment as comparison currently were as follows:

Firstly, in **Figure 5**&**6**, we have demonstrated the reliability and robustness of full-course non-invasive real-time NIR-II imaging and single-f-PDT step-by-step in comparison with the invasive surgery-like laser-assisted PDT using 5-ALA, which is currently a clinical therapy for the diagnosis and treatment of bladder cancer (*J. Urol.* 2001, 165, 1904–1907, Clinical trials number of NCT02101931). All data have confirmed the capability and superiority of full-course non-invasive real-time NIR-II imaging and single-f-PDT over traditional invasive treatment.

Secondly, we noticed that there still existed room to further improve it to relief repeated treatment in the clinic. Inspired by the clinical fractionated radiotherapy (f-RT, ref. 13 and 62), we thus proposed on-demand f-PDT with quantifiable imaging signal-to-background ratios (SBRs). However, the conventional small animal living imaging system failed to realize this purpose. Under this circumstance, we established a new system using a fast NIR photon counter and realized the quantification of real-time SBRs and on-demand f-PDT (**Figure 7**). The conclusions were in good consistency with the good standard H&E staining analysis and mutually corroborated with that in **Figure 5**&**6**. Multiple-comparison tests on the data shown in **Figure 7** were also found with significant differences. We thus concluded the reliability and robustness of the non-invasive real-time NIR-II imaging and on-demand f-PDT besides the non-invasive real-time NIR-II imaging and single-f-PDT.

Thirdly, we agreed with you and initially attempted to adopt traditional invasive treatment as a comparison in on-demand f-PDT, however, conventional modalities for bladder cancer imaging and treatment such as the invasive 5-ALA-based PDT could not emit NIR-II fluorescence to perform non-invasive real-time SBR quantification with either conventional or our new system. Meanwhile, the mice were also unable to receive at least one time a week the harmful bladder exposure and surgical suture as shown in **Supplementary Figure 19b**, thus restricting exact comparisons with on-demand f-PDT. Therefore, in consideration of the above reasons and animal rights and animal welfare, we did not conduct the less precise control experiments with traditional invasive treatment but designed two divergent clinical therapies in **Figure 7**.



Supplementary Figure 19 | b, Representative images of a bladder NMIBC mouse that reveal the protocol adopted in this study for surgery-like laser-assisted PDT (5-ALA+650-nm laser, 3 W).

Considering that no significant improvement on the diagnosis, treatment, and 5-year survival rates of bladder cancer has been achieved since the 1990s (*Nature* 2017, 551,

S34–S35), we would like to state that the whole process of non-invasive real-time NIR-II imaging and single-f-PDT as well as the on-demand f-PDT have extended the scope of current invasive imaging and therapeutic techniques with enhanced tumour regression, robust recurrence inhibition, and improved survival rates.

We acknowledge reviewer 2 for this rigorous concern and insightful suggestion and we believe that it would greatly help us further update our lab-made system, such as to integrate visible fluorescence imaging capture and quantification capability for traditional invasive treatment or further estimate comparison with traditional modalities with large animals that can tolerate repeated invasive treatment. We thank you for this inspiring suggestion again.

Reviewer #3 (Remarks to the Author):
I didn't have much time, but I think the manuscript/paper has potential. It's much too dense in its current format. Restructuring and focusing on the main findings in the main manuscript would really help. Interesting work, but the manuscript is very dense.

Overall response: We truly thank you for your valuable suggestion in your busy schedule that "*I think the manuscript/paper has potential, and "Interesting work*", we feel encouraged to establish this new nanotechnology-assisted approach toward the unmet clinical needs for non-invasive bladder cancer treatment.

We fully understand your kind concern that this manuscript was dense, as we also realized this issue. The manuscript was dense because it involved the following aspects that have never been reported previously, including the engineered nanoscintillators with concurrent X-ray-activated visible and NIR-II luminescence (**Figure 1**), the clinical alike carcinogen-induced NMIBC mouse models (**Figure 2**), in vitro cytotoxicity, specific cellular uptake, and cell-killing mechanisms of the proposed f-PDT (**Figure 3**&**4**), the superiority of non-invasive f-PDT over conventional invasive modality (**Figure 5**), the reliability of full-course real-time NIR-II imaging to non-invasively guide tumour development (**Figure 6**), and the concept of real-time imaging signal quantification and on-demand f-PDT with a lab-made multiple-excitation fast NIR photon counter system (**Figure 7**). All the figures have been organized in this logic to demonstrate the concept rigorously and clearly with more than 40 figures being supplemented in the Suppl. Info file. Extended Data Figures have been recognized in the Suppl. Info file. to keep the manuscript neat.

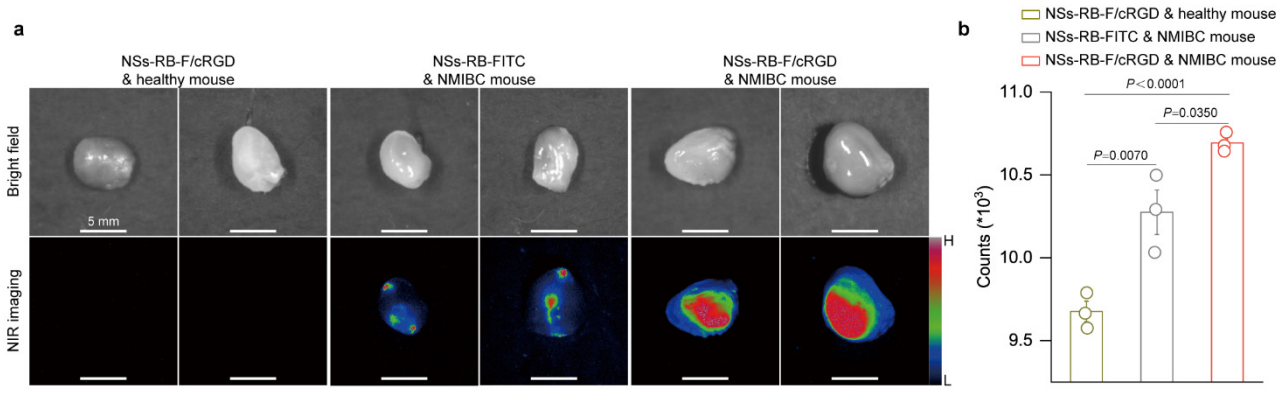
We understand that dense content would require more time to read and comprehend. However, considering the multidisciplinary terms in this manuscript, it might be more difficult to follow if some of the Figures (such as **Figures 3**&**4**) were placed in the Suppl. Info. file. For example, reviewer 2&4 recommended the comprehensive demonstration of cell-killing

mechanisms of the proposed f-PDT (·OH and $^1O_2$) to be important (comment 4 of reviewer 2 and comment 5 of reviewer 4). Under this circumstance, to make the contents more logic to broad audiences with different backgrounds, we maintained **Figures 3&4** in the main text and have revised the manuscript throughout as suggested by you and other reviewers. More details can be found as follows:

Comment 1: The targeting experiments are unconvincing, Figure 2f. The speculation about EPR effect doesn't make sense and the data are not properly quantified. It's unclear how many mice were included in anything related to Figure 2.
- For NIR imaging the tumor should be excised and shown, not merely the entire bladder.
- Flow cytometry experiments on digested tumors are required.
The requirement for RGD functionalization must be properly studied and substantiated. Neither is the need for FITC that is introduced with every RGD peptide.

Response: We appreciate your valuable suggestions on these issues. We have provided more data and evidence to support the EPR effect and the tumour targeting capability.

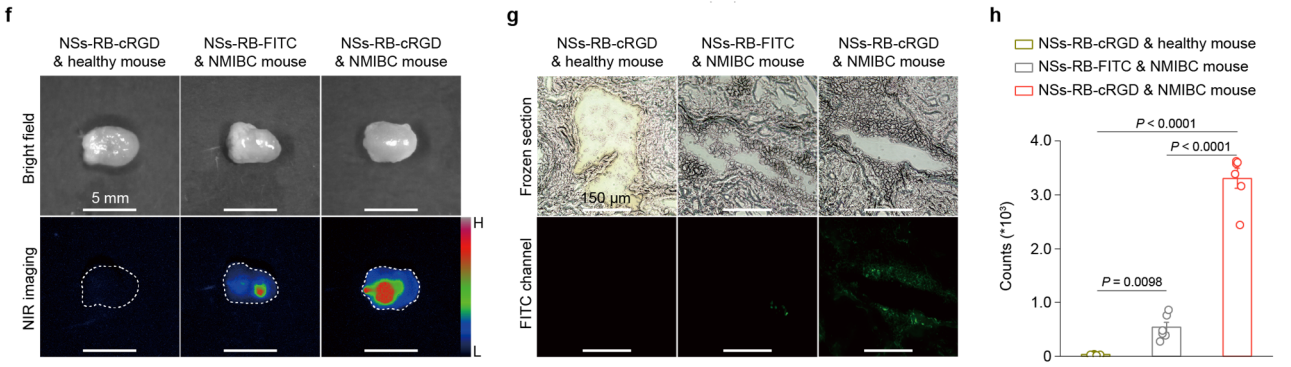
Firstly, as you inquired and were concerned about, we also treasure the robustness and reliability of data to support our conclusions. We did conduct parallel evaluations in all the experiments in **Figure 2**. Particularly, to demonstrate the successful establishment of NMIBC, we analyzed six randomly selected mice and all of them were observed with cancerous lesions after MNU instillation as shown in **Figure 2b** and **Supplementary Figure 8a**. In terms of the demonstration of the non-specific adsorption, the EPR effect, and the tumour-targeting capability, we analyzed three mice in each group, including those shown in **Figure 2f**, and the other parallel estimation and results that have been now provided in the revised manuscript as **Supplementary Figure 13**. All the data and results were in good consistency with that in **Figure 2f**, demonstrating the reproducibility of our protocol and conclusion. Moreover, to present ex vivo fluorescence imaging of these bladder tissues, we have also presented several corresponding frozen slices as shown in **Figure 2f** and **Supplementary Figure 8d-g** in the previous manuscript. We understand the importance of the robustness and reliability and would like to declare that for each experiment in **Figure 2** and the rest figures throughout the project we have conducted parallel estimations before drawing any conclusion.



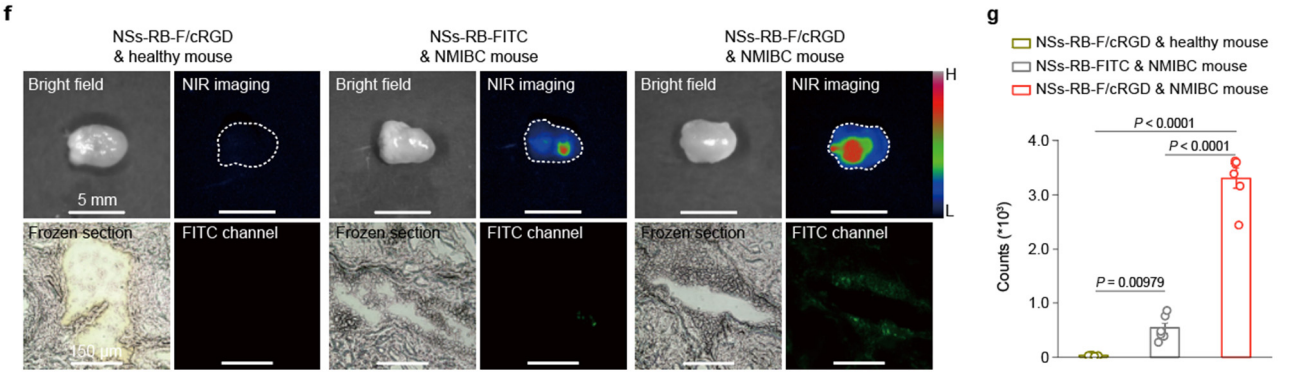
***New* Supplementary Figure 13 | a**, Ex vivo NIR-II fluorescence imaging (ex: 808 nm) of bladders dissected from the NSs-RB-F/cRGD-treated healthy mice and the NSs-RB-FITC-treated and NSs-RB-F/cRGD-treated NMIBC mice. **b**, Quantitative NIR-II fluorescence signals with statistical analysis in **a**. Data in **b** were shown as mean ± s.e.m. The *P* values in **b** were calculated by one-way ANOVA and Tukey multiple-comparison test.

Notably, as you may also find in **Figure 2f** and **Supplementary Figure 13** that the fluorescence distribution was like a single bright spot (as described by reviewer 2 in the comment 3), the reasons were as follows: (1) unlike **Figure 2b** that was taken with the inner surface of bladder tissues exposed initially to show the tumour lesions and successful establishment of NMIBC with no intravesical instillation of NSs-RB-F/cRGD, **Figure 2f** was taken from the original outer surface of bladder tissues that intravesically instilled with NSs-RB-FITC or NSs-RB-F/cRGD but not with the inner surface exposed to avoid detachment of tumour lesions considering that they were further employed to perform NIR-II fluorescence imaging with frozen slices (the original version of **Figure 2g** & **Supplementary Figure 8d-g**); (2) the urothelial carcinoma of the bladder is a typical multifocal papillary tumour as showed in **Figure 2b**, the different size of papillary tumours might lead to different accumulation amount of NSs-RB-F/cRGD with different NIR-II luminescence intensity in different parts of the tumour tissues as could be found in **Figure 2f**; (3) fluorescence imaging is commonly known to suffer from tissue scattering (*Nat. Biomed. Eng.* 2020, 4, 259–271; *Lancet Oncol.* 2019, 20, e354–67). Therefore, when bladder tissues are in their original state, one can image that the tumour lesions would condense and overlap, thus leading to the appearance of **Figure 2f** with "a single bright spot" as also shown in most in vivo or ex vivo fluorescence images and **Supplementary Figure 13** with a single large bright spot. To avoid possible misleading, we have emphasized the different states of tumour tissues in **Figure 2b** from "bladders externalized dissected" into "bladders externalized dissected (inner surface exposed)" in the revised manuscript with explanations as "…*Notably, the difference between the bright spots in Figure 2f and Supplementary Figure 13 and the diffusely distributed tumour lesions in Figure 2b was mainly because they were taken from different angles of view of bladders and the overlapping of tumour lesions when inside bladder tissue and also the tissue scattering of NIR-II fluorescence.*"

Secondly, the EPR effect was concluded not only by the ex vivo images of bladders in the original version of **Figure 2f** but also mutually supported by the results of the original version of **Figure 2g** and **Supplementary Figure 8d-g**, because the ex vivo NIR-II fluorescence imaging was conducted with the exactly the bladders shown in the original version of **Figure 2f**. Besides, all the healthy and NMIBC mice used for ex vivo imaging analysis received repeatedly intravesically instilled with PBS to wash out possible unaccumulated nanoparticles following 1 h after intravesical instillation of NSs-RB-FITC or NSs-RB-F/cRGD as demonstrated in the methods. To logically present the relationship between the bladder tissues and the corresponding frozen slices, we have also reorganized the original version of **Figure 2f** and original version of **Figure 2g,h** into a new version of **Figure 2f,g** in the revised manuscript.



The original version of **Figure 2 | f**, Ex vivo NIR-II fluorescence imaging (ex: 808 nm) of bladders dissected from the NSs-RB-F/cRGD-treated healthy mouse and the NSs-RB-FITC-treated and NSs-RB-F/cRGD-treated NMIBC mice. **g**, Fluorescence imaging of corresponding frozen slices (FITC channel, ex/em: 460-500/512-542 nm) of bladders dissected from the NSs-RB-F/cRGD-treated healthy mouse and the NSs-RB-FITC-treated and NSs-RB-F/cRGD-treated NMIBC mice. **h**, Quantitative FITC fluorescence signals with statistical analysis in **g**.



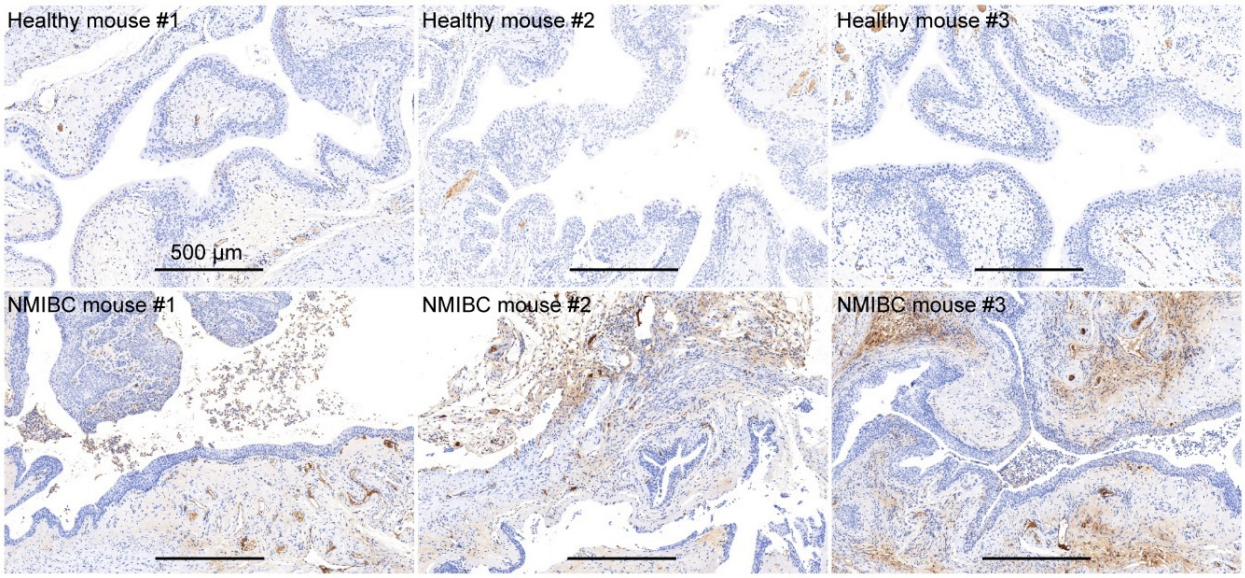
The revised new version of **Figure 2 | f**, Ex vivo NIR-II fluorescence imaging (ex: 808 nm) of bladders and the corresponding frozen slices (FITC channel, ex/em: 460-500/512-542 nm) that dissected from the NSs-RB-F/cRGD-treated healthy mouse and the NSs-RB-FITC-treated and NSs-RB-F/cRGD-treated NMIBC mice. **g**, Quantitative FITC fluorescence signals with statistical analysis on the corresponding frozen slices in **f**.

We would like to present why we demonstrated the EPR effect as well as the non-specific accumulation and tumour-targeting capability with the NMIBC mouse model (**Figure 2b** & **Supplementary Figure 13**), the corresponding frozen slices (**Figure 2f** & **Supplementary Figure 8d-g**), and the following extensive in vitro experiments (**Figure 2h-l**) in the previous manuscript:

(1) direct demonstration with NMIBC mouse model and the corresponding frozen slices: The mouse model has been recognized as the most convincing way to estimate in vivo behavior (e.g., *Nat. Nanotechnol.* 2021, 16, 266–276; *J. Am. Chem. Soc.* 2013, 135, 4978−4981; *Nat. Rev. Mater.* 2016, 1, 16014; *Proc. Natl. Acad. Sci. U.S.A.* 2016, 113, 11829−11834; *Sci. Adv.* 2023, 9, eabq8225; *Nat. Mater.* 2023, 22, 1421–1429).

Considering the clinical alike autochthonous bladder cancers have multiple subtypes, we therefore, first demonstrate with NMIBC mice. Briefly, the widely used tumour-homing cRGD peptides that can highly bind to the overexpressed integrin $\alpha_v\beta_3$ in tumour endothelium cells and bladder cancer cells were first modified onto the nanotransducers (ref. 27, 29 to 31). Therefore, after being washed with PBS for times, **Figure 2f** (left) with a rather low signal intensity in NSs-RB-cRGD-treated healthy mouse indicated barely any non-specific accumulation in healthy mouse bladder (or normal cells); **Figure 2f** (middle) with 20-times higher signals in NSs-RB-FITC-treated NMIBC mouse demonstrated passive targeting effect of non-cRGD-labelled nanotransducers, and **Figure 2f** (right) with more than 100-times higher signals in NSs-RB-cRGD-treated NMIBC mouse demonstrated active targeting effect of cRGD-labelled nanotransducers. Similar demonstrations and conclusions have also been shown in recent literature (*Nat. Mater.* 2023, 22, 1421–1429).

In support of the above conclusion, we have also conducted the immunohistochemistry (IHC) analysis with the bladder slices of three NMIBC mice and healthy mice, respectively, as suggested by reviewer 2 (comment 3). Briefly, as revealed in **Supplementary Figure 10**, $\alpha_v\beta_3$ integrin expression was observed highly expressed in the NMIBC bladder, compared to a rather low level in normal bladders. The results confirmed that after being washed with PBS, the accumulated nanotransducers in NMIBC were dominantly contributed by the high affinity of cRGD to $\alpha_v\beta_3$ integrin, whereas the one-hundredth signal in healthy mouse or the one-fifth signal could be inferred to be contributed by non-specific accumulation efficiency and the EPR effect.

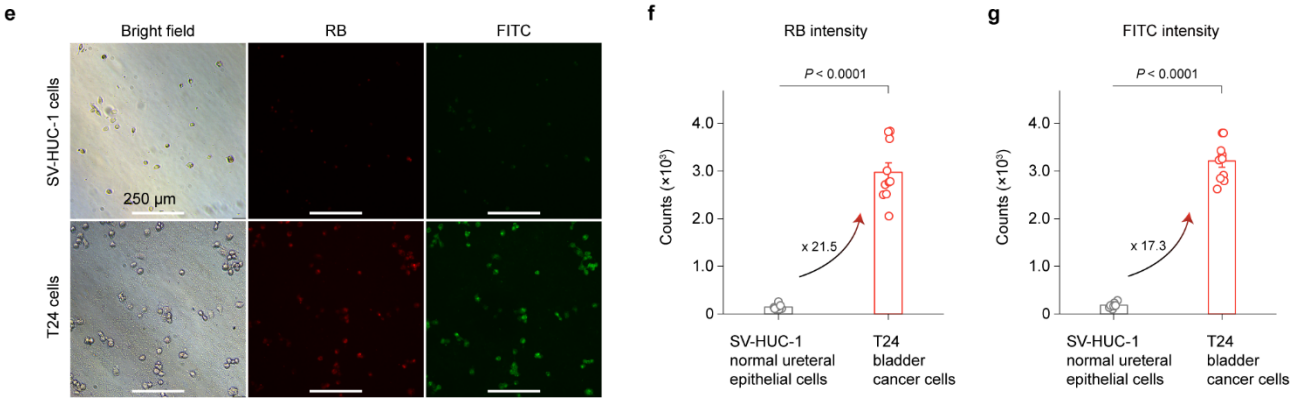


***New* Supplementary Figure 10 |** Expression of $\alpha_v\beta_3$ integrin in bladder tissues of NMIBC or healthy mice (Brown: $\alpha_v\beta_3$ Integrin-expressing cells; blue: nucleus).

(2) further demonstration with in vitro experiments: considering the feature and complexity of MNU-induced autochthonous bladder cancer, we adopted two human bladder cancer cell lines of T24 and 253J as representatives. Briefly, cellular uptake of NSs-RB-F/cRGD was found to be several times higher for both RB and FITC signals than that of NSs-RB-FITC

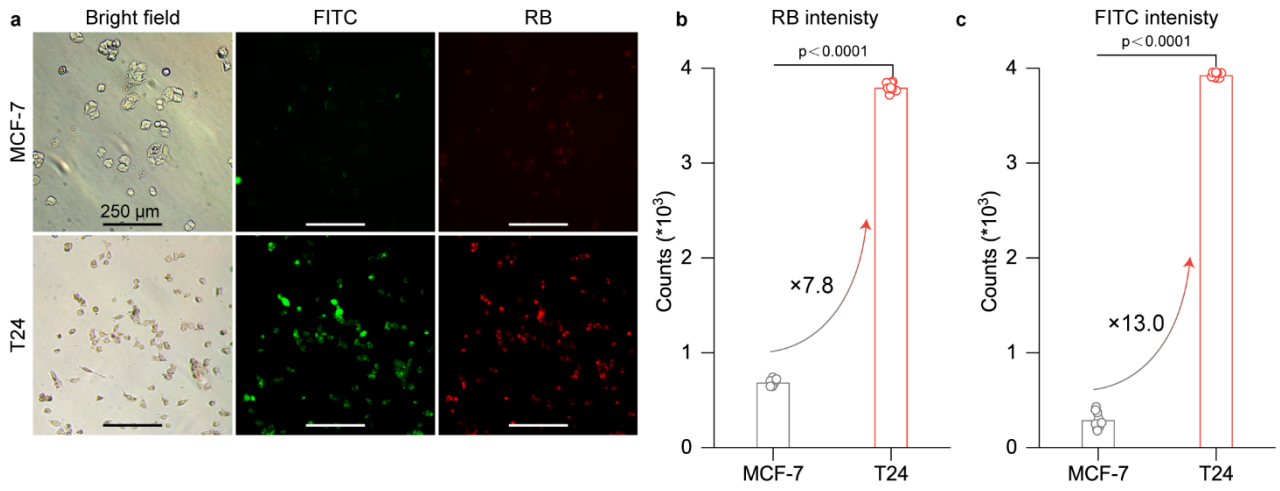
(**Figure 2h-l** & **Supplementary Figure 14a-d**), indicating the rationale of cRGD labeling onto nanotransducers towards clinical alike autochthonous bladder tumours.

In support of this conclusion, we also compared the uptake efficiency of NSs-RB-F/cRGD by the normal human urinary tract epithelial cells of SV-HUC-1 and the T24 cells in the previous manuscript. As shown in **Supplementary Figure 14e-g**, the RB and FITC intensities detected in T24 cells were about 20 times higher than that in SV-HUC-1 cells.



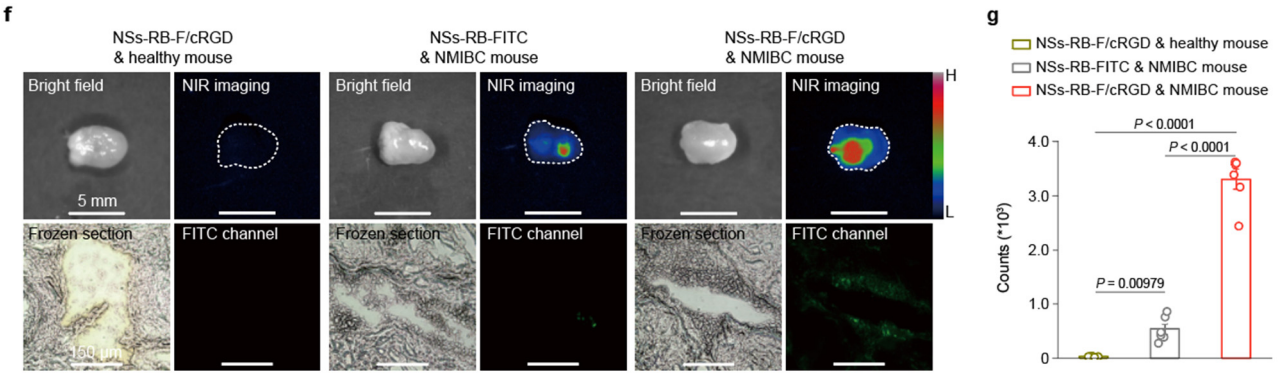
Supplementary Figure 14 | e,**f**,**g**, Fluorescence imaging (**e**) and quantitative RB (**f**) and FITC fluorescence intensities (**g**) in normal ureteral epithelial cells of SV-HUC-1 and bladder cancer cells of T24 incubated with NSs-RB-F/cRGD (50 μg mL^{-1}).

Moreover, we have also compared the uptake ability of NSs-RB-F/cRGD with tumour cell lines that have different expressions of $\alpha_v\beta_3$ integrin as suggested by reviewer 2 (comment 3). Briefly, as shown in **Supplementary Figure 16,** T24 cells with high $\alpha_v\beta_3$ integrin expression were found with much more intense RB and FITC signals with about 7.8 and 13.0-fold than that observed in MCF-7 cells with low $\alpha_v\beta_3$ integrin expression. These results indicated the amounts of $\alpha_v\beta_3$ integrin expression would affect the targeted uptake ability of NSs-RB-F/cRGD. Taken together, the conclusion that F/cRGD peptide modification improved the targeted uptake ability of NSs-RB-F/cRGD was again strengthened. We have added these new details in the revised manuscript "*Moreover, the RB and FITC intensities detected in breast cancer cells of MCF-7 with low $\alpha_v\beta_3$ integrin expression were much lower than those in bladder cancer cells of T24 with high $\alpha_v\beta_3$ integrin expression (Supplementary Figure 16), indicating the high affinity of F/cRGD peptides to overexpressed $\alpha_v\beta_3$ in NMIBC.*"

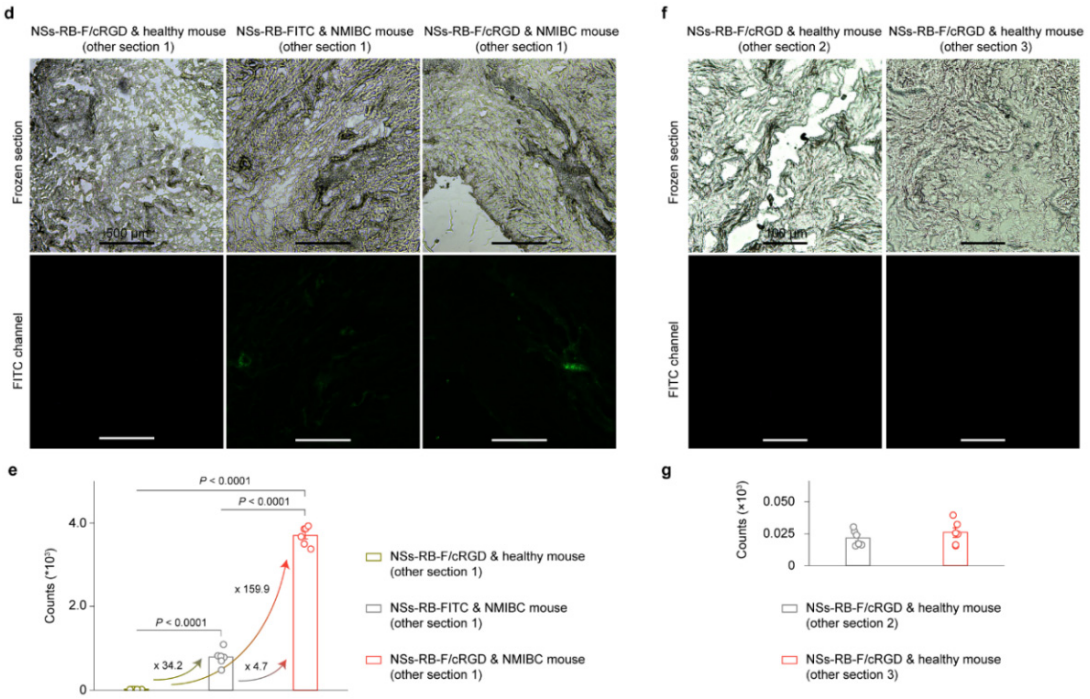


***New* Supplementary Figure 16 | a**,**b**,**c**, Fluorescence imaging (**a**) and quantitative RB (**b**) and FITC fluorescence intensities (**c**) in breast cancer cells of MCF-7 and bladder cancer cells of T24 incubated with NSs-RB-F/cRGD (50 μg mL^{-1}).

(3) In terms of "*For NIR imaging the tumor should be excised and shown, not merely the entire bladder*" and "*Flow cytometry experiments on digested tumors are required*", we agreed with you and appreciated this kind suggestion, which we initially attempted to conduct. However, unlike solid tumours, the specificity of NMIBC with multifocal papillary tumour lesions and carcinoma made it difficult to entirely excise the tumour from the bladder for NIR-II imaging and flow cytometry, and this is the dominating reason that bladder cancer tends to recur because transurethral resection of bladder tumour or endoscope techniques cannot eliminate all the lesions (*Nat. Rev. Urol.* 2022, 19, 280–294; *Nano Today* 2022, 45, 101551). Under this circumstance, instead of excising tumour tissues or collecting tumour lesions, we performed analysis on the frozen sections of the bladder (**Figure 2f**,**g** and **Supplementary Figure 8d-g** & **13**).

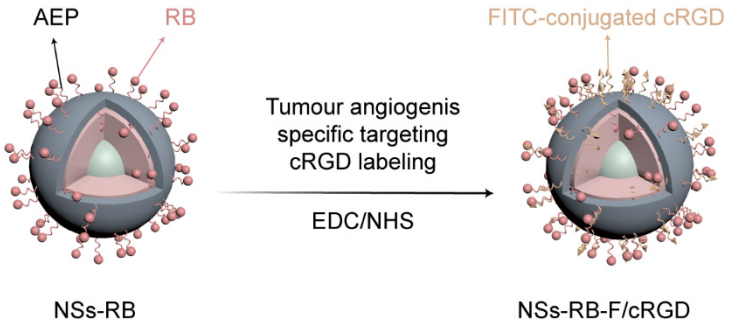


***The revised new version of* Figure 2 | f**, Ex vivo NIR-II fluorescence imaging (ex: 808 nm) of bladders and the corresponding frozen slices (FITC channel, ex/em: 460-500/512-542 nm) that dissected from the NSs-RB-F/cRGD-treated healthy mouse and the NSs-RB-FITC-treated and NSs-RB-F/cRGD-treated NMIBC mice. **g**, Quantitative FITC fluorescence signals with statistical analysis on the corresponding frozen slices in **f**.



Supplementary Figure 8 | d,**e**, Fluorescence imaging of frozen slices (FITC channel, ex/em: 460-500/512-542 nm) (**d**) and quantitative FITC fluorescence signals with statistical analysis (**e**) of dissected bladders from a healthy mouse infused with NSs-RB-cRGD and NMIBC mice infused with NSs-RB-FITC and NSs-RB-cRGD. **f**,**g**, Fluorescence imaging of frozen slices (FITC channel, ex/em: 460-500/512-542 nm) (**f**) and quantitative FITC fluorescence signals (**g**) in other two sections of the dissected bladder from the healthy mouse infused with NSs-RB-cRGD as control. Data in **e** and **g** were shown as mean ± s.e.m. The *P* values in **e** were calculated by one-way ANOVA and Fisher LSD multiple-comparison test.

(4) In terms of "*Neither is the need for FITC that is introduced with every RGD peptide*", we apologize for the confusion and misunderstanding caused by our description, as it was also pointed out by reviewer 1 (comments 5&6). In fact, cRGD-FITC (F/cRGD) peptide was purchased exactly as it was used to synthesize the target NSs-RB-F/cRGD from NSs-RB through the well-known NHS/EDC reaction. We did not label FITC onto cRGD by ourselves. To make the content clear, we have revised the expression of "NSs-RB-cRGD" into "NSs-RB-F/cRGD" in the revised **Figure 2c** & **2f,g,** and all other related figures throughout the manuscript.



***Revised* Figure 2 | c**, Surface functionalization of nanotransducers by cRGD-FITC (F/cRGD) peptides.

Comment 2: Figures 3&4 (data) can be moved to the Suppl. Info. The in vitro viability experiments are not informative (on potential tox and efficacy).

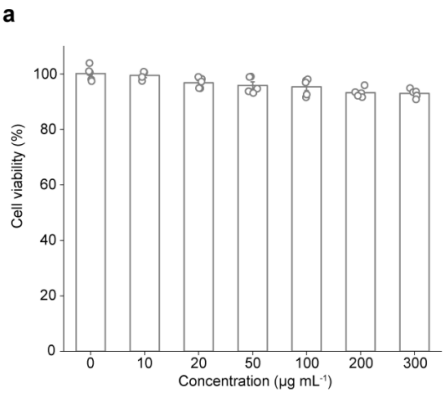
Response: We truly thank you for the kind suggestion and understand your concern about the dense contents in the manuscript, as we also realized this issue. As we have described that the content manuscript was dense, because it involved the following four aspects that have never been reported, including nanoscintillators with concurrent X-ray-activated visible and NIR-II luminescence (**Figure 1**), the clinical alike carcinogen-induced NMIBC models with tumour-targeting modification (**Figure 2**), in vitro cytotoxicity, specific cellular uptake, and cell-killing mechanisms of f-PDT (**Figure 3**&**4**), non-invasive f-PDT over conventional invasive modality (**Figure 5**), full-course real-time NIR-II imaging (**Figure 6**), and on-demand f-PDT with the lab-made multiple-excitation fast NIR photon counter system (**Figure 7**). All the main and supplementary figures were organized in this logic to make the content more comprehendible.

While **Figure 3**&**4** provided the pivotal information to understand the detailed mechanisms of the proposed f-PDT in the manuscript, you may also find that reviewer 2&4 recommended to provide more details on the cell-killing mechanisms of f-PDT (·OH and $^1O_2$) (comment 4 of reviewer 2 and comment 5 of reviewer 4). Under this circumstance, to make the contents more logic to broad audiences with different backgrounds, we maintained **Figure 3**&**4** in the main text, and we have also revised the manuscript throughout as you suggested. We hope you can understand this decision after careful consideration.

Notably, in terms of the "*The in vitro viability experiments are not informative (on potential tox and efficacy)*", we have provided more evidence to support the less cytotoxicity of NSs-RB-F/cRGD and their tumour treatment efficacy:

(1) in **Figure 3a**, the viabilities of T24 cells treated with NSs-AEP, NSs-RB, and NSs-RB-F/cRGD from 0 to 300 μg mL^{-1} were found to maintain at about 100%, indicating no obvious toxicity was induced to inhibit cell proliferation. Similarly, no obvious toxicity was observed in 253J (**Supplementary Figure 17b**), indicating the low potential toxicity of our target NSs-RB-F/cRGD (*Nat. Biomed. Eng.* 2022, 6, 144–156; *Nat. Commun.* 2022, 13, 509).

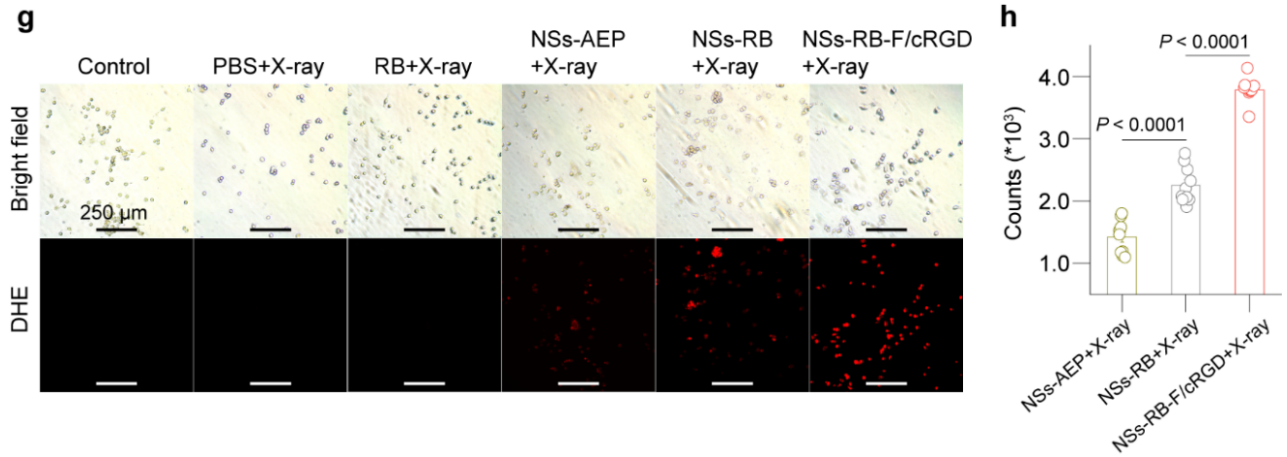
In support of the potential toxicity, we have also conducted the viability of normal human urinary tract epithelial cells of SV-HUC-1 to extend the potential toxicity estimation. As shown in **Supplementary Figure 17a**, no obvious cytotoxic was also observed in SV-HUC-1 cells. Therefore, we believed that the presented viability estimations with two cancer cells and one kind of normal cells could further strengthen the low potential toxicity of our proposed nanotransducers.



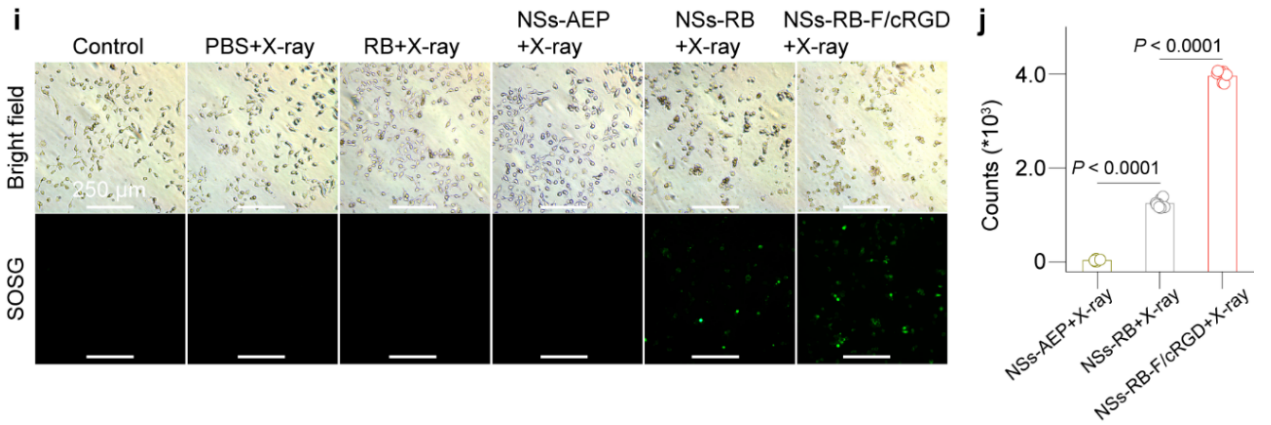
***New* Supplementary Figure 17 | a**, Viabilities of SV-HUC-1 cells after incubation with NSs-RB-F/cRGD at different concentrations.

(2) to demonstrate the efficiency of our target NSs-RB-F/cRGD, we first investigated the overall cytotoxicity under X-ray radiation at different doses or concentrations (**Figure 3b,c**), then studied the intrinsic radiosensitization effect of NSs (·OH) with clonal survival assay (**Figure 3d**) and DNA damage assays (**Figure 3e,f**) and the PDT activity of RB ($^1O_2$) with ROS estimation (**Figure 3g-j**), followed by the apoptotic process of tumour cells with Annexin V-APC/PI assay (**Figure 4a,b**), Western blotting (**Figure 4c,d**), and imaging flow cytometry (**Figure 4e**). Among all the experiments, parallel tests with multiple hypothesis testing have been conducted, and thus we concluded the high therapeutic efficiency of our target NSs-RB-F/cRGD.

(3) Notably, to emphasize the PDT activity, we have also performed the ROS generation estimation of our target NSs-RB-F/cRGD under X-rays as also suggested by reviewer 4 (comment 5). In brief, both the ·OH indicator of DHE and the $^1O_2$ indicator of SOSG were found with intense signals when treated with NSs-RB-F/cRGD, which further indicated the robustness of cell-killing efficiency of our proposed nanotransducers, as shown in the revised **Figure 3g,h** and the revised **Figure 3i,j**.



***Revised* Figure 3 | g,h**, Intracellular ROS imaging (DHE) (**g**) and signal quantification (**h**) of T24 cells that received different treatments under 1-Gy radiation (nanotransducers: 50 μg mL^{-1}).



***Revised* Figure 3 | i,j**, Intracellular $^1O_2$ imaging (SOSG) (**i**) and signal quantification (**j**) in T24 cells with different treatments under 1-Gy radiation (nanotransducers: 25 μg mL^{-1}).

Overall, based on the above evidence and data, we envisage that the potential toxicity of the proposed nanotransducers was low, while the cell-killing efficiency was relatively strong to finally achieve full-course NIR-II fluorescence imaging-guided f-PDT of autochthonous bladder cancer.

Comment 3: The data related to Figure 5 look clean and very promising. The subsequent experiments (Figure 6 & 7) are very difficult to follow and interpret. Why do NSs-RB-cRGD clear rapidly? Doesn't the targeting work?"

Response: We thank you for the positive comment "*The data related to Figure 5 look clean and very promising*" and are sorry that "*The subsequent experiments (Figure 6 & 7) are very difficult to follow and interpret*". We would like to introduce the content of Figure 6&7 in brief.

Firstly, as we have introduced the fact that no significant improvement on the diagnosis, treatment, and 5-year survival rates of bladder cancer have been achieved since the 1990s, with an unmet clinical need for non-invasive bladder cancer treatment, we thus proposed a full-course real-time imaging-guided on-demand f-PDT, and the content was presented in this logic:

(1) In **Figure 5**: we studied the therapeutic efficiency of NSs-RB-F/cRGD-based single-f-PDT with multiple control experiments including conventional invasive modality, and then conducted the good standard H&E staining of the collected bladder and spleen tissues of each group. The results demonstrated the superiority of our proposed concept.

(2) In **Figure 6**, we established a non-invasive technique to monitor tumour development based on the NIR-II fluorescence of NSs-RB-F/cRGD, and then to employ the established imaging technique to predict the tumour recurrence. Briefly, we found that the detected NIR-II fluorescence signals indeed reflected the tendency of tumour regression or progression in mostly NMIBC mice that has been evidenced by the good standard H&E staining analysis, thus demonstrating the convincing non-invasive imaging modality. We then employed the

imaging technique to further monitor tumour development within a 3-time longer period than the standard treatment period, and the deduction of whether recur or not was mutually validated by H&E staining results. Therefore, we established a convincing and robust non-invasive full-course real-time imaging for bladder cancer.

(3) In **Figure 7**, we were to further propose a concept to on-demand adjust practical radiation doses based on the advantages of non-invasive full-course real-time imaging in monitoring tumour development, which also has not been introduced in the field. However, to achieve this, we must first build a new system with a fast NIR photon counter to quantify signal-to-background ratios (SBRs) of NIR-II fluorescence signals immediately during the treatment process. Finally, through a list of experiments, we realized the integration of full-course real-time NIR-II imaging and on-demand f-PDT.

Overall, from **Figure 5** to **Figure 6** to **Figure 7**, we step by step demonstrated the robustness of f-PDT, full-course real-time NIR-II imaging, and the full-course real-time NIR-II imaging-guided on-demand f-PDT, all of which have never been reported by far. We envisage that these results would inspire the field with more clinically promising technologies, and we hope you could understand why the contents must be presented such densely to make it solid.

Secondly, in terms of rapid clearance of NSs-RB-cRGD presented in the manuscript and supported by **Supplementary Figure 26**, the reasons were mainly as follows:

(1) in our work to perform NIR-II fluorescence imaging and f-PDT, at each time point NSs-RB-F/cRGD was intravesically instilled into bladders for 1 h followed by perfusion of PBS to wash out untargeted nanotransducers.

(2) the accumulated NSs-RB-F/cRGD in NMIBC was mainly contributed by the high affinity of cRGD to the overexpressed integrin $\alpha_v\beta_3$. Literature has reported that peptides of RGD or cRGD (cyclic RGD) would degrade by proteases in the body (*Chem. Eng. J.* 2022, 450 138004; *Bioorg. Med. Chem.* 2012, 20, 2549-2557; *Biomacromolecules* 2015, 16, 2701-2714; *Langmuir* 2019, 35, 1273-1283; *Cancer Med.* 2024, 13, e6800) within 12 hours. Therefore, the short half-life of cRGD would lead to the gradual clearance of accumulated NSs-RB-F/cRGD.

(3) as we have explained in response to comment 5 of reviewer 2 that unlike solid tumours or tumours in other organs, necrotic bladder tumour cells are rapidly cleared out from the body through urine (*Clin. Transl. Disc.* 2023, 3, e183) and urinary exfoliated tumour cell is widely used in the diagnosis of bladder cancer in the clinic (*Nat. Rev. Urol.* 2023, 20, 597–614; *Br. J. Cancer* 2014, 130, 369–379), therefore, the gradual cell death and tumour necrosis would also lead to the clearance of NSs-RB-F/cRGD from the NMIBC mice.

Therefore, due to the above reasons, NSs-RB-F/cRGD would be gradually cleared out of the body. We would like to declare that the residence time of NSs-RB-F/cRGD in NMIBC for

12 h at each time point was sufficient to perform all the imaging and treatment procedures. Meanwhile, the clearance of NSs-RB-F/cRGD from the body could also help avoid long-term toxicity, which was beneficial for further clinical translation.

Reviewer #4 (Remarks to the Author):
Reviewer summary: The authors synthesize novel nanotransducers that can be activated by x-ray or laser to emit in the visible and near-infrared regions. These nanotransducers are conjugated with peptides that specifically bind to tumor cells. Following activation by external x-rays, these compounds result in increased tumor cell killing and improved survival of mice bearing NMIBC tumors. Using infrared imaging, tumors can be non-invasively monitored after treatment.

The work addresses a significant clinical problem, as NMIBC is common and frequently recurs following treatment. Furthermore, disease monitoring currently requires cystoscopy/biopsy, which is invasive and is imperfect at estimating disease burden and extent. On the technical side, I have some significant questions and potential concerns regarding the autochthonous model used extensively in this work. On the conceptual side, the need for relatively high-dose radiation to activate the compound is somewhat unattractive, as radiation can be associated with short and long-term toxicity, which are often acceptable when radiation is being used as the therapeutic modality, but which seem more difficult to accept when radiation is being used as the activator of the compound rather than as a therapy unto itself.

- What are the noteworthy results?
Overall, this is a comprehensive study of x-ray activated nanoparticle photodynamic therapy for the treatment of bladder cancer. The theory behind x-ray activated photodynamic therapy is explained in Figure 1a/b. The remainder of Figure 1 delineates the specific spectral qualities of the nanoparticle components. The authors showed the specific in vivo uptake of the nanotransducers into bladder tumor cells in Figure 2, which gives evidence for its use as an imaging modality. Figure 3 and 4 show the specific cytotoxic effects of x-ray activated in vitro in bladder cancer cells. Figure 5 describes the in vivo effects of photodynamic therapy in MNU-induced NMIBC mouse models. Figure 6 and Figure 7 shows the post-operative monitoring capabilities of the nanoparticle technology.

- Will the work be of significance to the field and related fields? How does it compare to the established literature? If the work is not original, please provide relevant references.
Photodynamic therapy is an active area in bladder cancer research. Clinical trials are ongoing to best determine its role in standard treatment, especially of non-muscle invasive

disease (NMIBC). Overall, the results of this manuscript provide evidence for the feasibility of coupling a novel technology (i.e. photodynamic therapy) with radiation for the treatment of NMIBC. Detecting recurrence is a challenging clinical paradigm in the treatment of NMIBC and requires frequent invasive cystoscopies and trips to the OR. Regimens which may enhance the sensitivity of cystoscopic evaluation of NMIBC are needed, and this could be one of those regimens.

- Does the work support the conclusions and claims, or is additional evidence needed?
In order to enhance the author's claims of the nanoscintillator technology efficacy in the treatment of NMIBC, further studies may be needed in a more clinically relevant setting. For example, combination therapy with either BCG or other standard-of-care intra-vesical therapy or ADCs could provide the basis for clinical trials alone. Currently, combination treatment with RT alone would not be feasible treatment regimen. In vivo experiments which include a combination with gem/cis and/or immunotherapy could be an appropriate treatment environment (i.e. tri-modal therapy) and efficacy in this setting would be a stronger clinical correlate.

- Are there any flaws in the data analysis, interpretation and conclusions? - Do these prohibit publication or require revision?
Please see detailed comments and requested edits below.

- Is the methodology sound? Does the work meet the expected standards in your field?
The authors chose a carcinogen-induced model of bladder cancer in mice, which is a reasonable and well-established approach. They use this model as a proxy for NMIBC. The authors include both in vitro and in vivo experimental approaches, which are both a standard and necessary to show pre-clinical efficacy. Various relatively simple staining (IHC, imaging, and FACS-based) assays are used to support the author's conclusions, and these are mostly clearly presented in the figures and text.

- Is there enough detail provided in the methods for the work to be reproduced?
While I am not an expert in the development of these x-ray nanoparticles, the rationale behind their use is sound and the protocols for their development appear reproducible. The mouse experiments are certainly feasible and reproducible. The staining assays are also relatively simple and could be easily reproduced.

Overall response: We truly thank you for highly approving our scope and manuscript that "*The work addresses a significant clinical problem*",
"*…this could be one of those regimens*", "*this is a comprehensive study of x-ray activated nanoparticle photodynamic therapy for the treatment of bladder cancer*",
"*…the results of this manuscript provide evidence for the feasibility of coupling a novel technology (i.e. photodynamic therapy) with radiation for the treatment of NMIBC*",
"*…a carcinogen-induced model of bladder cancer in mice, which is a reasonable and well-established approach…both in vitro and in vivo experimental approaches, which are both a standard and necessary to show pre-clinical efficacy. Various relatively simple staining (IHC,*

imaging, and FACS-based) assays are used to support the author's conclusions, and these are mostly clearly presented in the figures and text",
and "*the rationale behind their use is sound and the protocols for their development appear reproducible. The mouse experiments are certainly feasible and reproducible. The staining assays are also relatively simple and could be easily reproduced*", as you are also aware that "*…NMIBC is common and frequently recurs following treatment. Furthermore, disease monitoring currently requires cystoscopy/biopsy, which is invasive and is imperfect at estimating disease burden and extent*",
"*Photodynamic therapy is an active area in bladder cancer research. Clinical trials are ongoing to best determine its role in standard treatment, especially of non-muscle invasive disease (NMIBC)*",
and "*Detecting recurrence is a challenging clinical paradigm in the treatment of NMIBC and requires frequent invasive cystoscopies and trips to the OR*". We feel encouraged to further promote such concept and their use in real clinical scenarios.

We truly appreciate your insightful suggestions to further extend the clinical values of this concept, which are of great significance to our research orientation and the fields of bladder cancer and nanomedicine.

Briefly, (1) regarding the comment on the autochthonous model, we have added more data and analysis and strengthened the conclusions (see responses to comment 2, 3, 6, and 9 for more details); (2) regarding the issue of relatively high-dose radiation, we have provided the effective dose received by the mouse was as low as 0.047 Gy as only the pelvis area was exposed to X-rays when using the traditional X-ray irradiator (160 kV, 250 mA) despite the use of a radiation dose of 4 or 6 Gy with a scheme illustrating the procedure (see responses to comment 7 for more details); and (3) regarding the suggested combination treatment with BCG or other standard-of-care intra-vesical therapy or ADCs or other gem/cis and/or immunotherapy, we would like to clarify that the proposed technique realized enhanced tumour regression, robust recurrence inhibition, improved survival rates, and accompanied NIR-II imaging non-invasively compared to the clinically approved invasive cystoscopy-assisted 5-ALA-based phototherapy, while it only required X-ray irradiation. Therefore, we envisage that such a simple and efficient nanotechnology possesses huge potential for further clinical translation.

Overall, we truly thank you for your affirmation of our concept and all the critical comments, which indeed helped us evaluate our manuscript and concept to be more encouraging, and we would like to emphasize that the proposed full-course real-time NIR-II imaging-guided on-demand therapy has never been described before, and we are conducting ongoing work to highlight X-ray-activated simultaneous imaging and therapy of progressive bladder cancer and demonstrating their therapeutic efficiency with large animals.

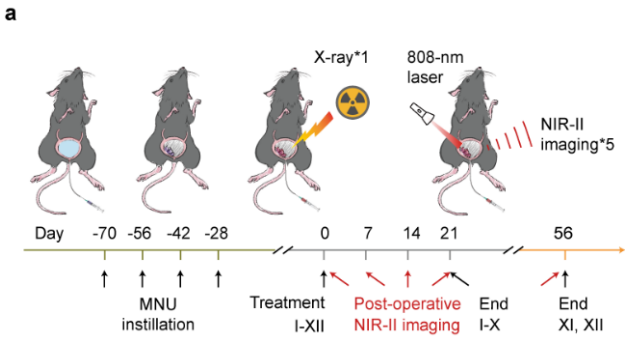
Comment 1: Additional description of Rose Bengal (RB) is required

Response: We appreciate your valuable suggestion on this issue, which would help broader audiences to comprehend the content. We have added more descriptions on this issue in the revised manuscript as "*…by covalent conjugation of Rose Bengal (RB) as photosensitizers onto... RB is a typical synthetic fluorescein derivative that efficiently generates $^1O_2$ under excitation at 500-600 nm.*"

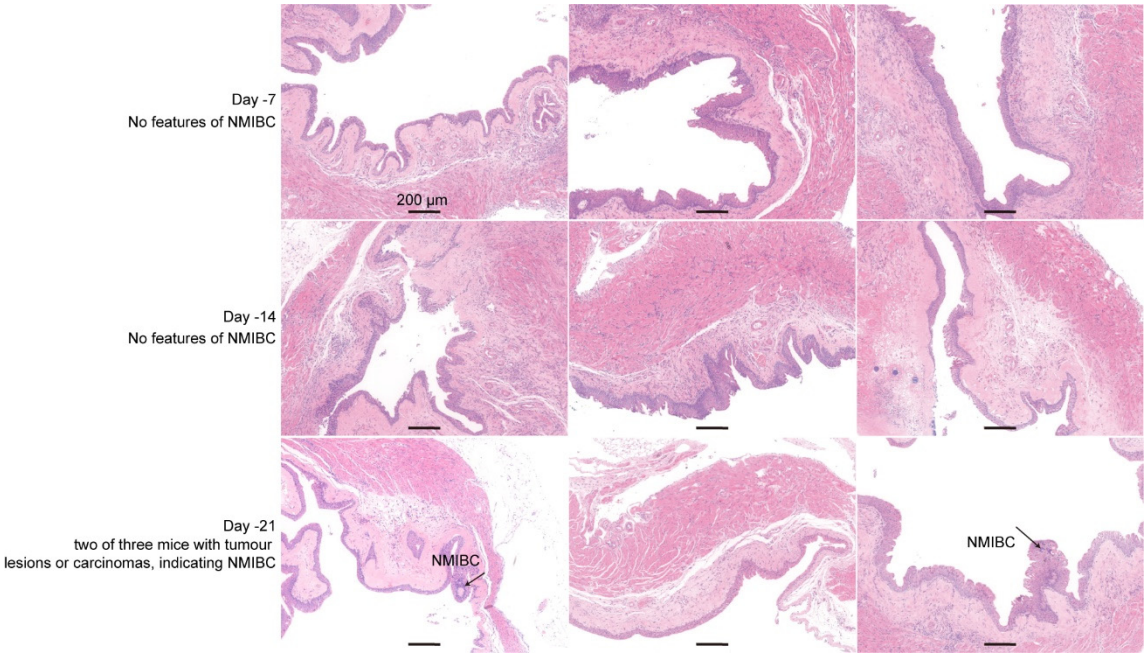
Comment 2: For the MNU mouse model in Fig 2A, how were mice monitored for tumor formation? (ultra-sound? MRI?). When were mice sacrificed relative to MNU treatment start date and/or date of first tumor formation?

Response: We thank you for the valuable comment and understand your concern on this issue, as the successful and reproducible establishment of the autochthonous model is crucial to this whole project. In 2015, the co-corresponding author Dr. Guoliang Yang from Renji Hospital reported the protocol to construct the MNU-induced animal model (*J. Exp. Clin. Canc. Res.* 2015, 34, 77), which was adopted by other researchers (e.g., *Adv. Sci.* 2018, 5, 1800004; *Oncotarget* 2016, 7, 28235-28246.). Moreover, the feasibility of the MNU-induced mouse model has also been recommended in other groups (*Nat. Rev. Cancer* 2015, 15, 42–54; *BMC Cancer* 2016, 16, 422; *J. Phys. Conf. Ser.* 2019, 1323, 012020; and *Eur. J. Pharm. Biopharm.* 2020, 151, 162–170). We therefore adopted this protocol in our project.

In brief, as shown in Methods and **Figure 5a**, the establishment of NMIBC was determined with preliminary experiments, the protocols were to first intravesically instill MNU solution via epidural catheter within 30 min every other week for a total of four times (marked as -70, -56, -42, and -28 day). Following each MNU instillation, mice were kept sedated for at least 60 min to prevent spontaneous urination of MNU, and then conducted H&E staining of tumour slices at -21, -14, -7 (**Supplementary Figure 7**) and 0 day (**Figure 2b** and **Supplementary Figure 8**) to estimate the appearance of NMIBC with three randomly selected mice at the first three time points and six at day 0 (not too early to be with only few carcinomas nor too late to be MIBC or even metastasis). Therefore, the time point of four weeks after the last intravesical instillation of MNU was used as the treatment beginning time when we conducted the extensive experiments in this project with randomly assigned experimental groups. Among all the processes of the mouse model, the good standard H&E staining was adopted as the most dominating convincing evidence as it has been widely used in the clinic and the above-mentioned literature. We thank you for the suggestion of ultrasound or MRI and would like to adopt them in the ongoing research with large animals.



***Revised* Figure 5 | a**, Schematic illustration of the establishment of NMIBC mouse models and experimental protocols for single-f-PDT.



***New* Supplementary Figure 7** | H&E staining results of bladder from mice that received the fourth MNU instillation (namely day -28 as shown in Figure 5) for 7 days (marked as day -21 according to Figure 5a), 14 days (marked as day -14), and 21 days (marked as day -7), which indicated that at day -7, two of the three randomly selected mice were detected with apparent appearance of tumour carcinomas in the bladder.

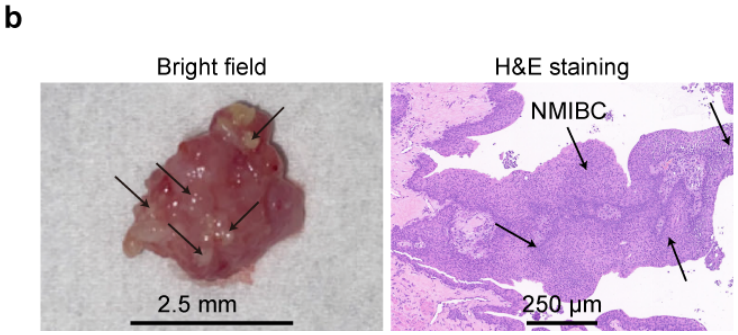
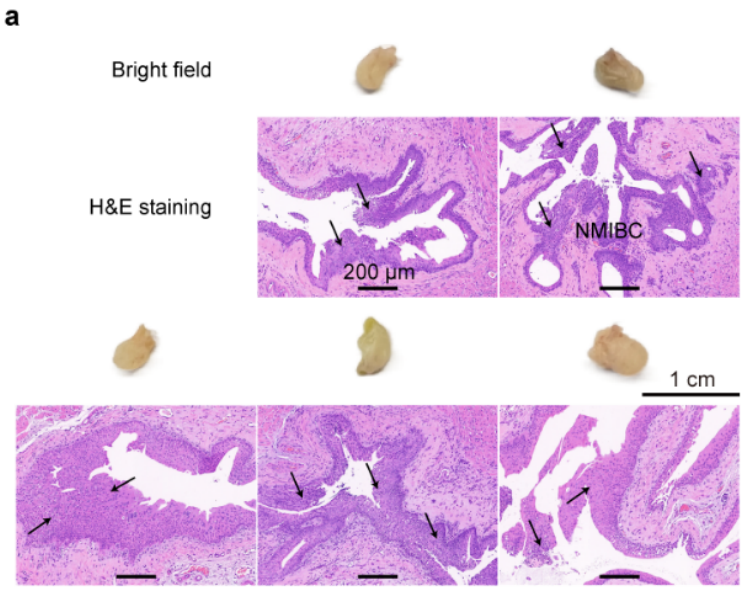


Figure 2 | b, A representative photograph and H&E staining image of the bladder from a NMIBC mouse after MNU instillation. Black arrows: carcinomas.



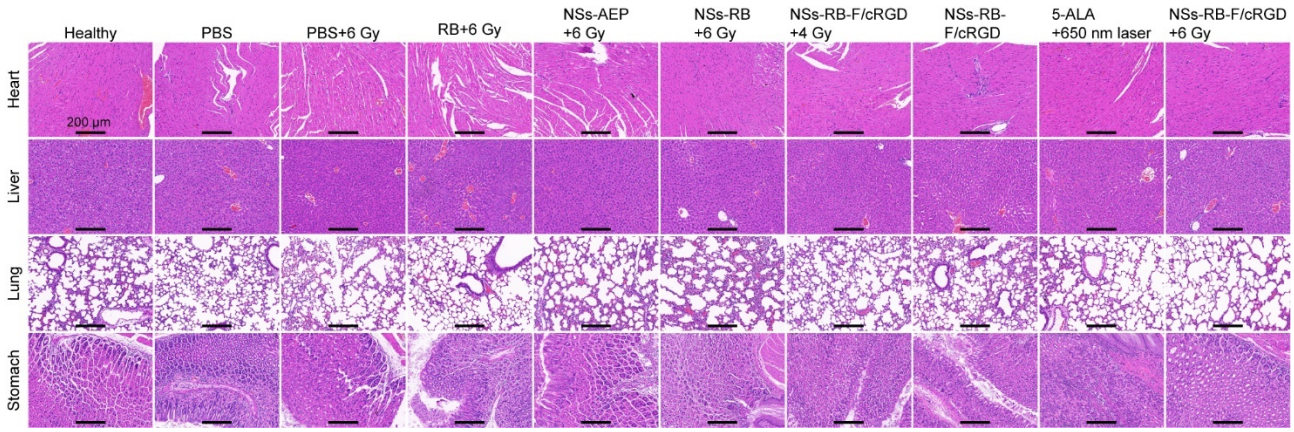
Supplementary Figure 1 | Photographs (top) and corresponding H&E staining images (bottom) of dissected bladders from five MNU-induced autochthonous bladder tumour mice. Black arrows: NMIBC regions.

Based on the above detailed described protocol and procedure for constructing NMIBC, we set the fourth week after mice received the fourth MNU instillation as the time to conduct in vivo experiments (marked as day 0). Therefore, the time that mice were sacrificed relative to the MNU treatment start date was day 21 in **Figure 5** for group I-X to demonstrate the therapeutic efficacy of single-f-PDT and day 56 to further monitor whether NMIBC would recur with an extra period of 35 days. For on-demand f-PDT in **Figure 7**, the time was also day 56 to maintain consistency.

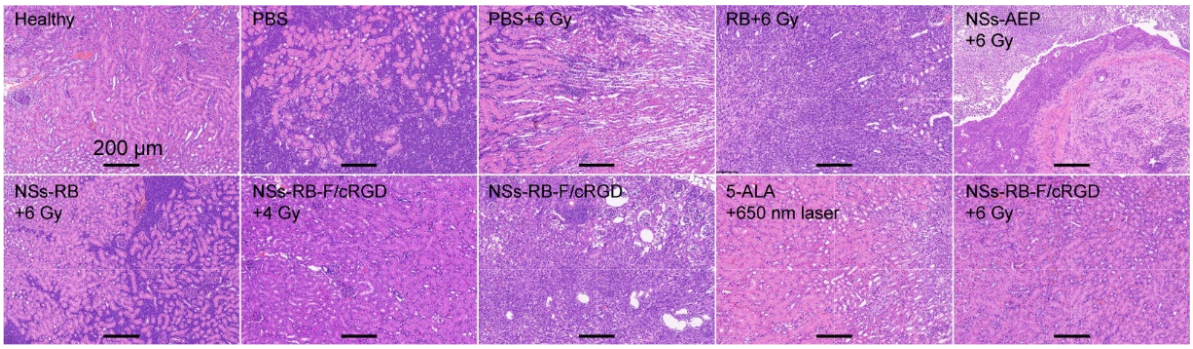
We have also added the H&E staining images obtained at day -21, -14, and -7 in the revised manuscript as **Supplementary Figure 7** to help broad audiences better understand this clinical alike autochthonous bladder mouse model.

Comment 3: It would be worth mentioning if there were any metastasis at any point prior to Day 56 in the mouse experiments (as the lack of metastasis would support its utility as a model of NMIBC).

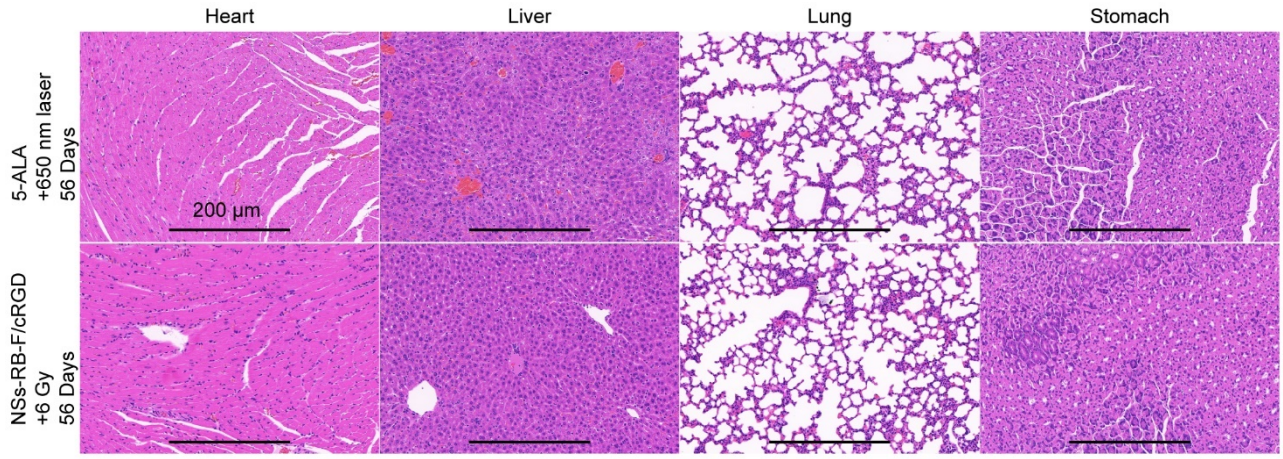
Response: We thank you for the logical and valuable suggestion. We were also serious about this important issue and tracked tumour development during the whole project. We observed no metastasis among all the survived mice of group I-X that sacrificed at day 21 and of group IX-IIX at day 56 in **Figure 5** based on the H&E staining (**Supplementary Figures 22, 30 & 31**, **Supplementary Figures 23 & 27**), and the dead mouse at day 31 and all the remaining nine mice at day 56 in **Figure 7 and Supplementary Figure 37** & **39**. The above results indicated the utility of all the mice as the exact model of NMIBC, as no signs of bladder cancer metastasizing to the major organs (heart, liver, lung, kidneys, and stomach).



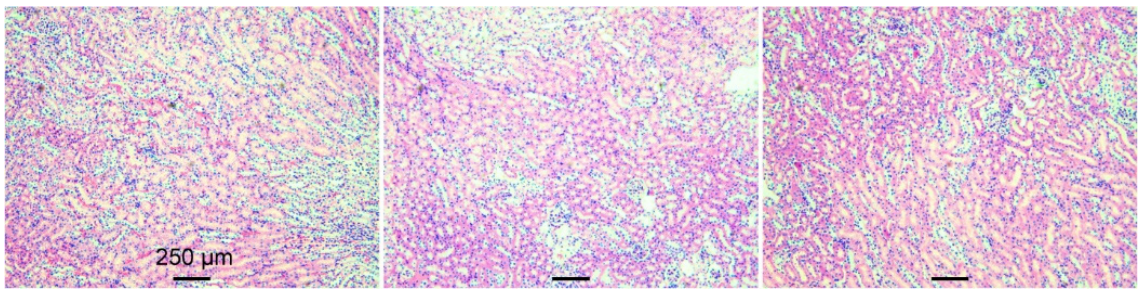
***New* Supplementary Figure 23 |** H&E staining images of major organs (heart, liver, lung and stomach) from NMIBC mice receiving different treatments at Day 21, showing no abnormal or metastasis signature.



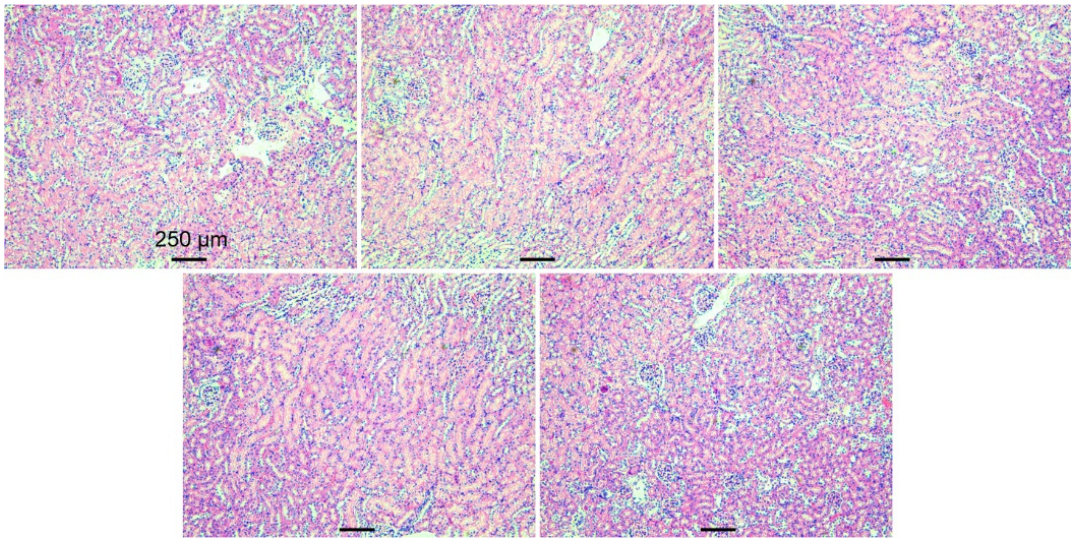
Supplementary Figure 22 | Representative H&E staining images of kidneys dissected from different treatment groups at day 21.



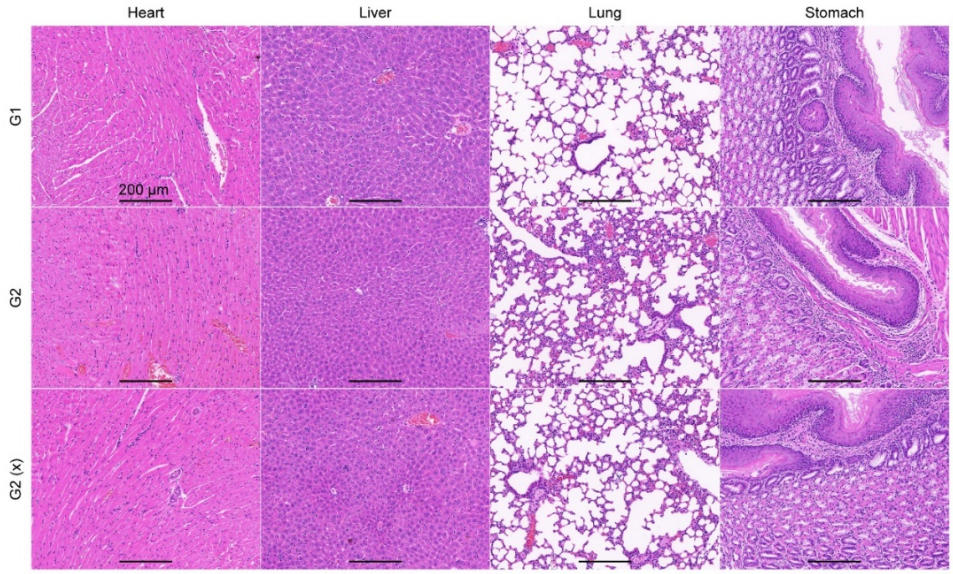
***New* Supplementary Figure 27 |** H&E staining images of major organs (heart, liver, lung and stomachs) from NMIBC mice receiving different treatments at Day 56, showing no abnormal or metastasis signature.



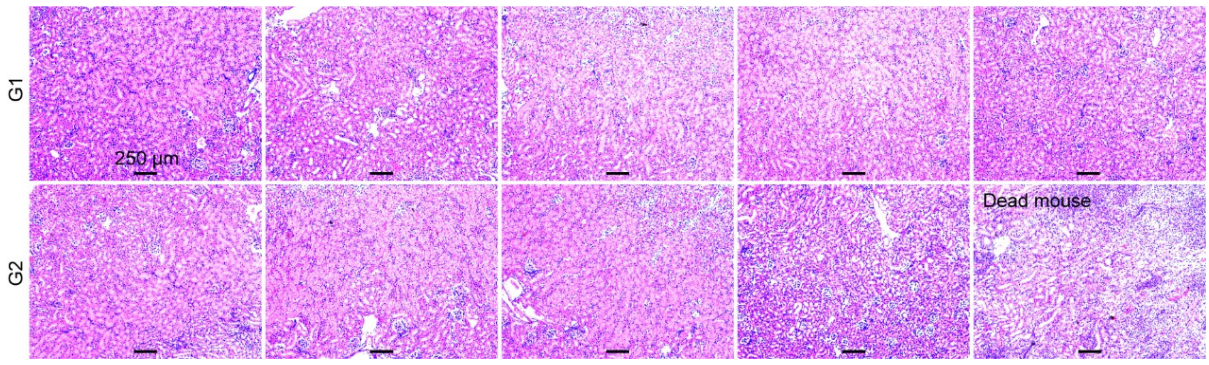
Supplementary Figure 30 | H&E staining images of kidneys dissected from the three remaining mice receiving treatment of 5-ALA+laser (XI group: 5-ALA+650 nm laser, 56 Day).



Supplementary Figure 31 | H&E staining of kidneys dissected from the five remaining mice receiving treatment of NSs-RB-F/cRGD+6 Gy (XII group: NSs-RB-F/cRGD+6 Gy, 56 Day).



***New* Supplementary Figure 39 |** H&E staining images of major organs (heart, liver, lung, and stomachs) dissected from mice in G1 and G2 at day 56 and G2(x) at day 31, showing no abnormal or metastasis signature.



Supplementary Figure 37 | H&E staining of kidneys dissected from the nine remaining mice at day 56 and the mouse died at day 31.

It has also been reported that in the clinic approximately 75% of all bladder cancer patients are diagnosed to be NMIBC at initial diagnosis, and metastasis is not unusual in NMIBC (*World J. Surg. Onc.* 2022, 20, 226), we inferred that this might be the reason that no metastasis happened during our project. Meanwhile, the diagnostic standard for NMIBC, MIBC, or metastasis is determined with the assistance of a trained pathologist. We have added the above data in the revised manuscript to support our conclusion as "*Mice treated with NSs-RB-F/cRGD+6 Gy and 5-ALA+laser were also observed with no significant abnormalities in the dissected organs, which indicated no metastasis occurred (Supplementary Figure 21-23).*"

Comment 4: For experiment summarized in Figure 2F-G, why was NSs-RB-FITC not shown in healthy mice?

Response: We thank you for this valuable comment on this issue. As you may realize **Figure 2f,g** was designed to investigate the contribution of F/cRGD peptides on the tumour-targeting capability and accumulation efficiency of nanotransducers, and NSs-RB-FITC was utilized as control.

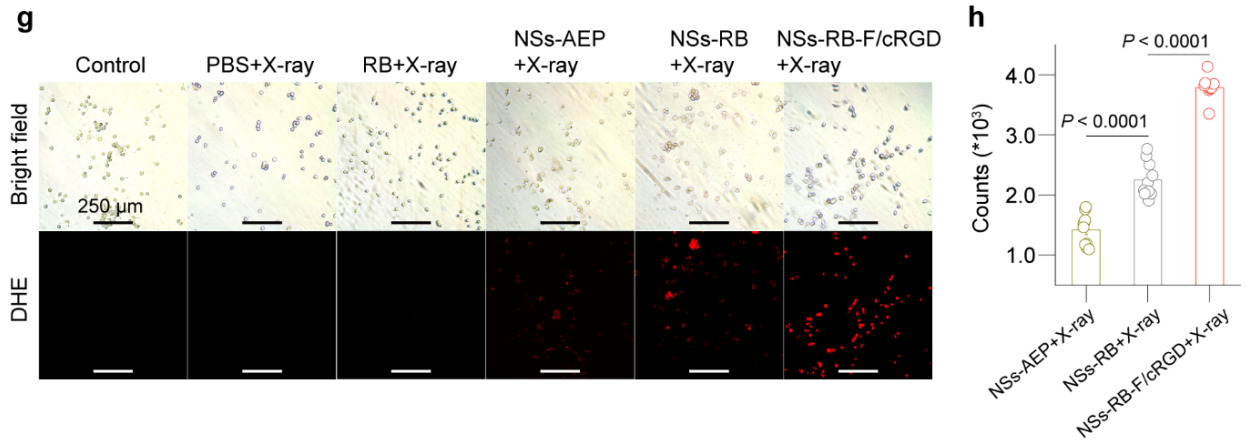
Considering the tumour-targeting capability of F/cRGD peptides was its high affinity for the overexpressed integrin $\alpha_V\beta_3$, and normal bladder tissues or cells express low level of integrin $\alpha_V\beta_3$ (*Biomaterials* 2021, 264, 120434; *Nat. Mater.* 2023, 22, 1421–1429), therefore, whether the modification of cRGD or not would not lead to tumour-targeting capability or high tumour accumulation in normal tissues or cells. And even if cRGD indeed contributed to the tumour-targeting or accumulation, the intensity of the FITC signal with NSs-RB-F/cRGD would be higher than that with NSs-RB-FITC. However, as shown in **Figure 2f,g**, the intensities of NSs-RB-F/cRGD-treated healthy mice were less than one hundredth that of NSs-RB-F/cRGD-treated NMIBC mice. Under this circumstance, we did not investigate NSs-RB-FITC treatment in healthy mice. We thank you for this suggestion and will conduct such complete investigations in the ongoing research.

Comment 5: For experiments summarized in Figure 3G-J, why was NSs-RB-cRGD + x-ray not tested? Is it because the ROS assay relies on fluorescence readout that would be obscure by FITC-labeled cRGD? If so, this should be stated explicitly, and a ROS assay that does not rely on fluorescence readout should be considered so that the NSs-RB-cRGD

compound can be tested and its impact on ROS generation compared to other compounds (NSs-AEP and NSs-RB) since it seems like the authors believe that NSs-RB-cRGD is the 'lead compound' at this point based on its superior properties.

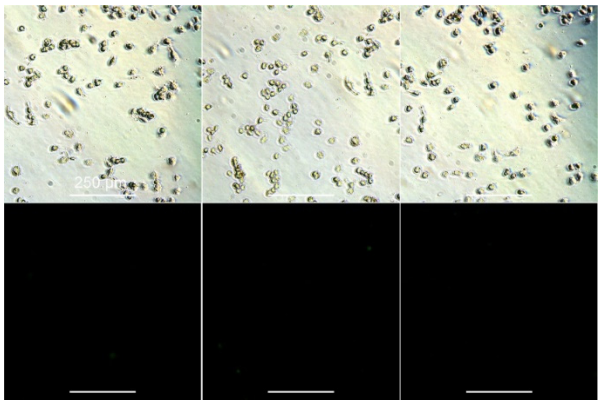
Response: We appreciate this careful logic and indeed the fluorescence of FITC would affect the fluorescence of DCFH-DA and SOSG in the ROS assays, therefore, NSs-RB was used to estimate ROS generation in the previous manuscript.

To directly demonstrate the superior properties of the 'lead compound' of NSs-RB-F/cRGD, we utilized dihydroethidium (DHE) that emits red light under 535 nm excitation as the ROS indicator (*Front. Bioeng. Biotechnol.* 2022, 10, 829868; *Nat. Commun.* 2023, 14, 1401). As shown in **Figure 3g**,**h**, the cells after incubated with NSs-RB-F/cRGD + X-ray were found to exhibit intense fluorescence signals, which was also slightly higher than that with NSs-RB + X-ray or NSs-AEP + X-ray, indicating that the superior ROS generation of NSs-RB-F/cRGD with enhanced cellular uptake.

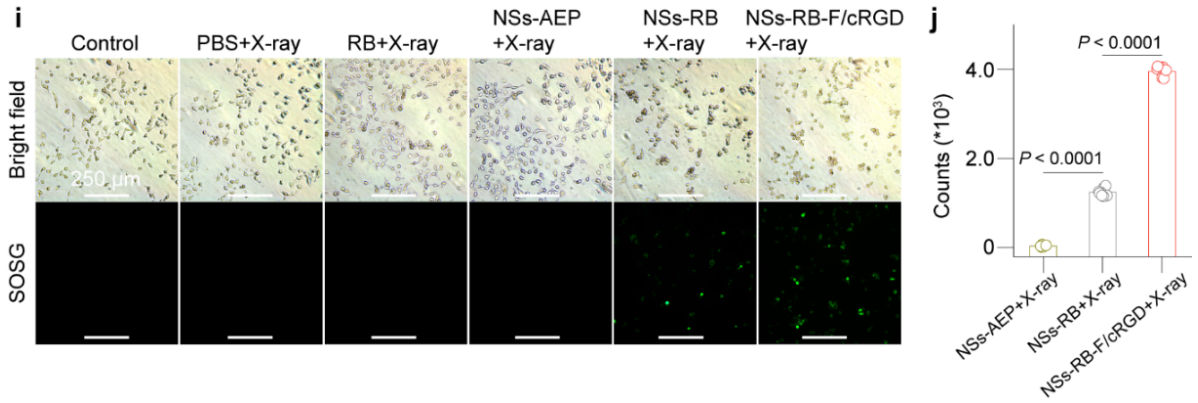


***Revised* Figure 3 | g**,**h**, Intracellular ROS imaging (DHE) (**g**) and signal quantification (**h**) of T24 cells that received different treatments under 1-Gy radiation (nanotransducers: 50 μg mL^{-1}).

Moreover, to directly demonstrate the superior properties of the 'lead compound' of NSs-RB-F/cRGD in generation $^1O_2$, we utilized half of its concentration of 50 ug mL^{-1} that was widely used among other in vitro studies and found that FITC fluorescence of F/cRGD peptides could not be detected at 25 μg mL^{-1} (**Response Figure 1**), indicating that it would not affect the SOSG assays. As shown in **Figure 3i**,**j**, the cells after incubated with NSs-RB-F/cRGD at 25 μg mL^{-1} and irradiated with 1-Gy X-rays exhibited intense fluorescence signals with the values to be slightly higher than that of NSs-RB + X-ray, while cells treated with NSs-AEP + X-ray showed no signals. Together with the results, the feature of the radiosensitization effect of NSs and the photodynamic activity of RB in generating ROS in our 'lead compound' of NSs-RB-F/cRGD could be demonstrated. We have added these data in the revised manuscript as the new version of **Figure 3g,h** and **Figure 3i,j**.



***Response* Figure 1 |** Fluorescence imaging (FITC fluorescence) T24 cells incubated with NSs-RB-F/cRGD (25 μg mL^{-1}).



***Revised* Figure 3 | i,j**, Intracellular $^1O_2$ imaging (SOSG) (**i**) and signal quantification (**j**) in T24 cells with different treatments under 1-Gy radiation (nanotransducers: 25 μg mL^{-1}).

Comment 6: Additional details regarding the tumor model used for the efficacy studies in Figure 5 are required. How are mice monitored for tumor formation following MNU administration? What is the cause of death in mice that die during the experiment? It is somewhat surprising to me that all mice appear to be randomized at day 70 following MNU administration, and then ~50% are dead within 10 days after randomization. This would suggest that the system is incredibly uniform and predictable in its behavior if all mice have equivalent tumors and are reasonably healthy at 70 days, but then many die within the next 10 days if untreated. Most autochthonous models display significantly more heterogeneity in terms of time to tumor development and survival after developing tumors. Details regarding cause of death (or criteria for sacrifice) are particularly critical when attempting to interpret data from this experiment.

Response: We truly thank you for your kind reminder on this issue. We apologize for the confusion caused by our expressions and lack of a more detailed description, which is crucial for the audience to comprehensively understand our design and results.

Regarding the monitoring of tumour formation following MNU administration, we adopted the good standard H&E staining of bladders from randomized three or six mice at day 7, 14,

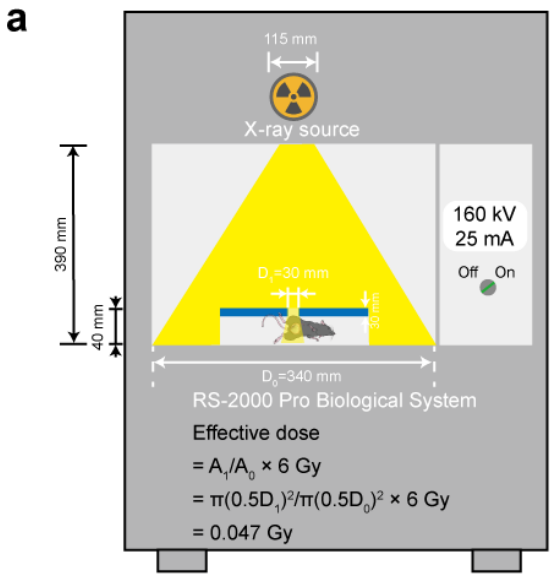
21, and 28 after the fourth MNU administration that was performed once every two weeks. According to our previous protocol and similar literature, it took about 42 days to finish MNU administration and additional 28 days to monitor tumour development. As we found that on the 63rd day about two-thirds of the mice appeared with NMIBC, and on the 70th day all six randomly selected mice were found with NMIBC, we made the 70th day the first day to start MNU administration in the whole project (**Figure 5**, marked as day 0, and thus marked the first MNU administration time as day -70). To estimate the therapeutic effect or confirm the reliability of NIR-II imaging, we also adopted good standard H&E staining with the assistance of a trained pathologist (see comment 2 for more details).

Regarding the cause recording of death in mice during the experiment, we indeed adopted a combination standard of either real death caused by tumours or the criteria for sacrifice caused by heavy tumour burden. Since two-thirds of mice appeared with NMIBC at day 63 and all mice with NMIBC at day 70, we observed in our preliminary experiments that some mice after the experiment began would gradually appear signatures of being lethargic with poor appetite and limited mobility, and then their weight would drop from initial ~22 g to about ~15 g due to the rapid tumour progress of NMIBC. Moreover, mice suffering from these signatures usually died within 1~2 days, and once the mice died their bladder tissues would be hard to collect with intact tumour lesions for H&E staining analysis. We therefore determined the standard of either real death or the criteria for sacrifice with the above signatures, as also with the consideration of animal rights and animal welfare. Notably, despite such quick heavy tumour burden was not extensively observed in subcutaneous tumor models, there also existed a similar criterion for sacrifice by recording mice with tumour volumes more than 2000 mm^3 to be dead (*Lab Anim.* 2022, 51, 208–209). We envisage that with a larger number of mice in each group with precise control of autochthonous animal models to achieve minimum clinical important difference (MCID), conclusions with more informative details would be obtained. We thank you for this valuable reminder, and we have added these details and the standard in the Method to help a broad audience better understand our project and the feature of bladder cancers as "*Notably, to record the death of mice during the treatment, a combination standard of either real death caused by tumours or the criteria for sacrifice caused by heavy tumour burden with the signatures including being lethargic, poor appetite, limited mobility, and/or weight dropping to about 15 g based on consideration of animal rights and animal welfare and data collection for analysis.*"

Comment 7: How were x-ray treatments delivered? Were these image-guided treatments or was the entire mouse (or entire pelvis) irradiated? What beam arrangement and RT planning parameters were used?

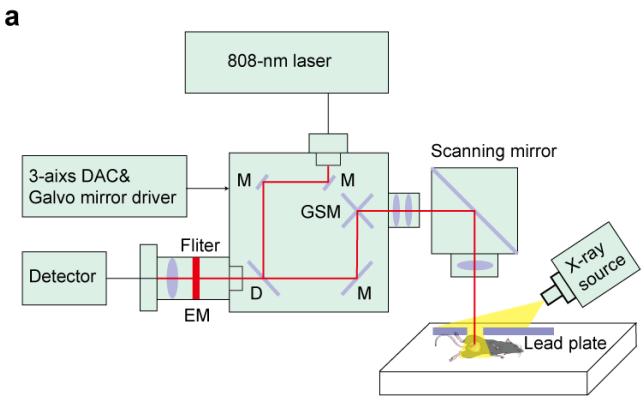
Response: We thank you for this valuable suggestion. All mice exposed to X-ray radiation were covered with a 30 mm-thick lead plate for protection with only the pelvis area exposed to X-rays.

Briefly, for single-f-PDT in **Figure 5**, mice were irradiated with the commercially available X-ray irradiator (RS 2000 Pro, Rad Source) at parameters of 160 kV and 250 mA with the beam dose rate to be 1 Gy/min. The total radiation dose of 4 or 6 Gy was performed with irradiation for 4 and 6 mins. Therefore, as shown by the scheme in **Supplementary Figure 19a**, the effective dose by the pelvis area was estimated to be as low as about 0.047 Gy. We have added the illustration and scheme in the revised manuscript and the Method part as "*The X-ray source-to-surface distance was measured as 390 mm with a circular irradiation area (D= 340 mm). A 30 mm-thick lead plate was used to shield the mice with only the pelvis area exposed through a hole to receive X-ray radiation. X-ray beams were generated by the commercially available X-ray irradiator (RS 2000 Pro, Rad Source) at parameters of 160 kV and 250 mA with the beam dose rate to be 1 Gy/min.*"



***New* Supplementary Figure 19 | a**, X-Ray machine used for therapy given to mice and relevant geometrical parameters.

Similarly, for on-demand f-PDT in **Figure 7**, mice were irradiated with our lab-built system equipped with an X-ray tube (VJ X-ray, China) at parameters of 70 kV and 80 mA with the beam dose rate to be 0.025 Gy/min as measured by a dosimeter. The total radiation dose of 1 or 3 Gy was performed with irradiation for 40 or 120 mins. We have also added these details in the revised manuscript and the Method part "*The X-ray source-to-surface distance was measured as 150 mm with a circular irradiation area (D= 100 mm). A 30 mm-thick lead plate was used to shield the mice with only the pelvis area exposed through a hole to receive X-ray radiation. X-ray beams were generated by the commercially available X-ray irradiator (VJ X-ray, China) at parameters of 70 kV and 80 mA with the beam dose rate estimated to be 0.025 Gy/min.*" We have also re-drawn the scheme in **Figure 7a** to provide these details.

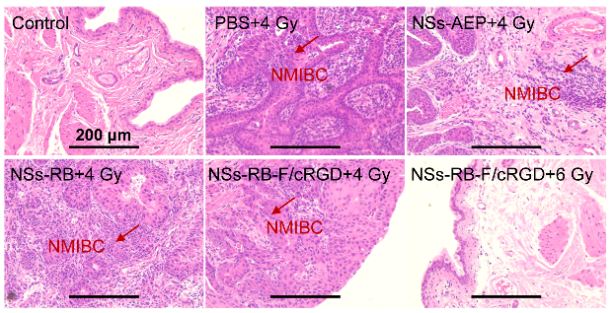


***Revised* Figure 7 | a**, Scheme of our lab-made system (M: mirror; D: dichroic mirror; GSM: Galvo scanning mirror; EM: emission).

Comment 8: Do the authors believe that the improved mouse survival observed with NSs-RB-cRGD plus 6 Gy compared to 4 Gy is due to the increased RT dose or increased efficacy of the NSs-RB-cRGD following excitation with 6 vs 4 Gy? It may be difficult to know because a control arm of PBS + 4 Gy was not included.

Response: We appreciate this kind and insightful concern and apologize for this confusion. However, we would like to state that we did not intend to draw a conclusion between NSs-RB-F/cRGD plus 6 Gy with that plus 4 Gy, the in vivo experiments were mainly designed to study and compare the therapeutic efficiency of proposed non-invasive f-PDT with that of invasive surgery-like PDT based on 5-ALA plus laser. NSs-RB-F/cRGD plus 4 Gy and all the rest control experiments were to provide more data, details, and evidence to help better understand the features of the proposed f-PDT. In fact, the dose of 6 Gy was determined from the preliminary experiment before the formal experiment (**Response Figure 2**).

Group	MNU-Induced	Materials	Radiation dose	Sacrifice Time
I	No	PBS	0	21 d
II	Yes	PBS	4 Gy	21 d
III	Yes	NSs-AEP	4 Gy	21 d
IV	Yes	NSs-RB	4 Gy	21 d
V	Yes	NSs-RB-F/cRGD	4 Gy	21 d
VI	Yes	NSs-RB-F/cRGD	6 Gy	21 d



***Response* Figure 2 |** Grouping information and H&E staining results of the preliminary experiment.

We hence deduced that the leading reason for the improved mouse survival between NSs-RB-F/cRGD plus 6 Gy with that plus 4 Gy should be the increased RT, namely the radiosensitization effect. The reasons were as follows: (1) tumours are generally hypoxic, the intrinsic radiosensitization effect to generate ·OH was independent of oxygen concentration within the tumour microenvironment and constant, while the f-PDT activity to generate $^1O_2$ relied completely on oxygen concentration and would gradually slow down with the consumption of oxygen. Therefore, with the increasing radiation time at 1 Gy/min, it could be inferred that the radiosensitization effect would maintain its therapeutic contributions compared to the f-PDT effect; (2) our deduction was also supported by the in vitro experiments, as it could be found that with increasing the radiation dose or time, the tendencies of the decreases in cell viabilities between both T24 and 253J cells treated with NSs-AEP and NSs-RB were similar (**Figure 3b-d** & **Supplementary Figure 17c,e,f**); (3) the fact that the efficiency of PDT relied completely on oxygen amounts was the leading reason in the field of anticancer to develop non-oxygen-dependent or extra oxygen generation or co-delivery strategies whether excited by X-rays or conventional lasers (*Nat. Rev. Cancer* 2003, 3, 380-387; *Nat. Commun.* 2022, 13, 2225; *Angew. Chem. Int. Ed.* 2015, 54, 1770-1774; *Nano Lett.* 2018, 18, 9, 5768-5774; *ACS Nano* 2021, 15, 11112-11125). Notably, despite the different contributions by radiosensitization effect and f-PDT activities, we would like to declare that both contributions were achieved by one nanocomposite and the convenient and non-invasive single X-rays and realized enhanced tumour regression, robust recurrence inhibition, and improved survival rates compared to traditional invasive strategies.

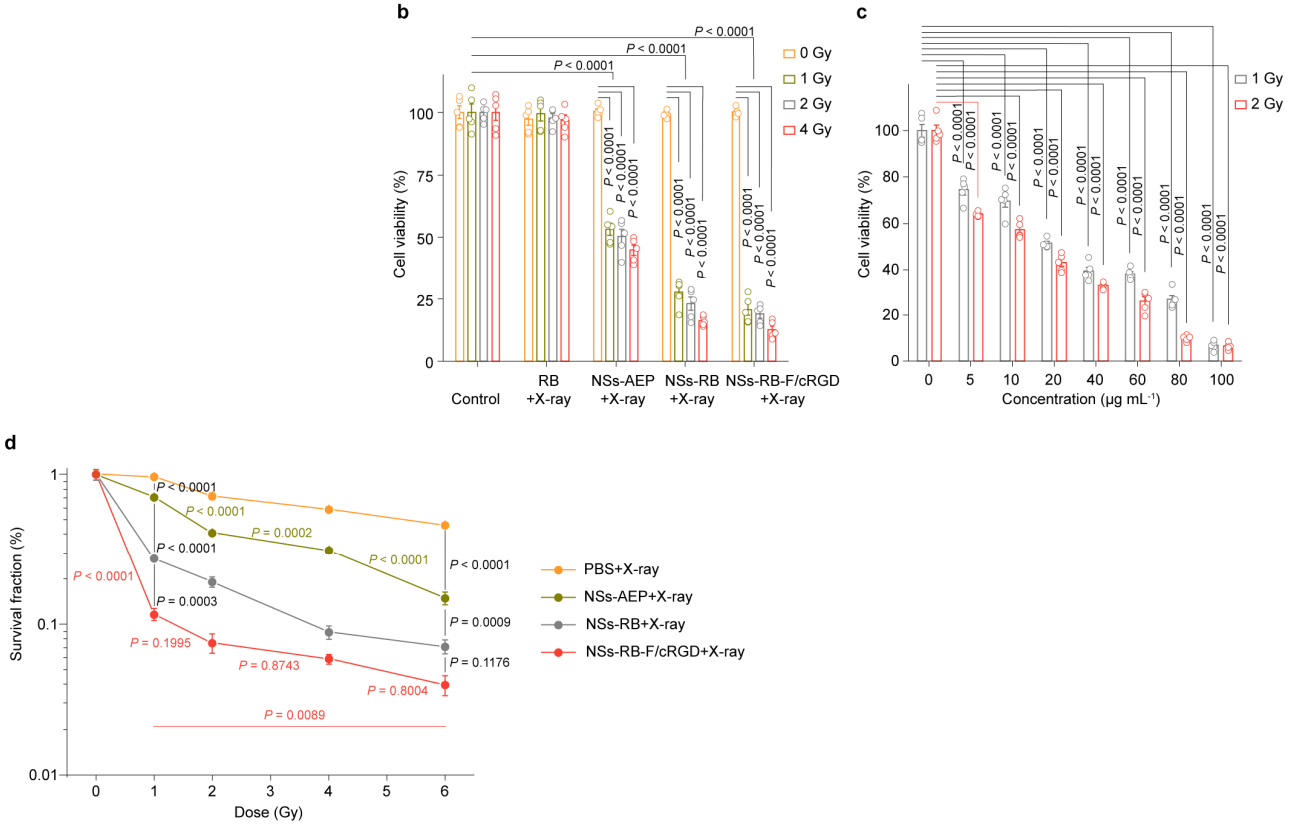


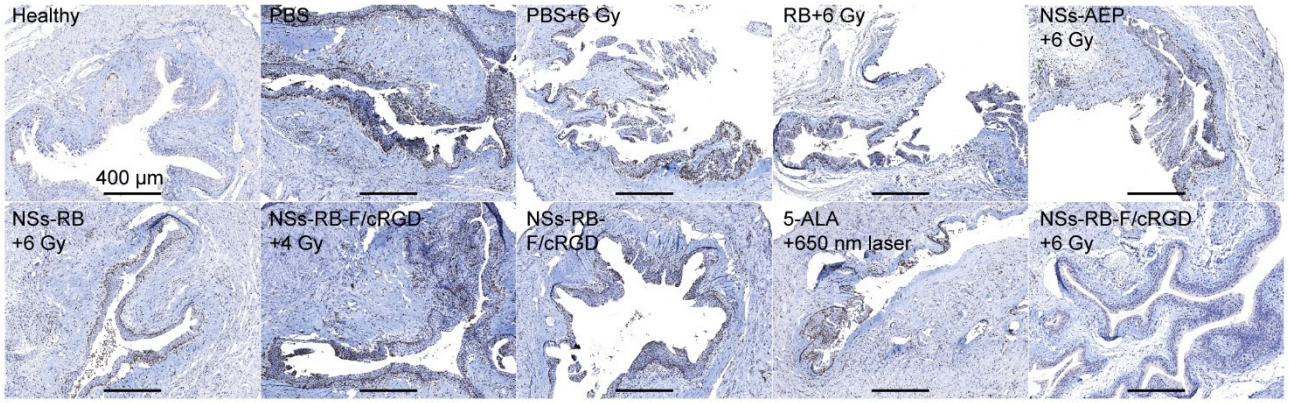
Figure 3 | b, Viabilities of T24 cells treated with RB, NSs-AEP, NSs-RB, and NSs-RB-cRGD with X-ray irradiation at 0, 1, 2, and 4 Gy (nanotransducers: 50 μg mL^{-1}). **c**, Viabilities of T24 cells treated with NSs-RB-cRGD at different concentrations and X-ray doses. **d**, Survival fractions of T24 cells incubated with NSs-AEP, NSs-RB, and NSs-RB-cRGD under various

X-ray doses (50 μg mL^{-1}). Data in **b**, **c**, and **d** were shown as mean ± s.e.m. The *P* values in **b**, **c**, and **d** were calculated by one-way ANOVA and Tukey multiple-comparison test.

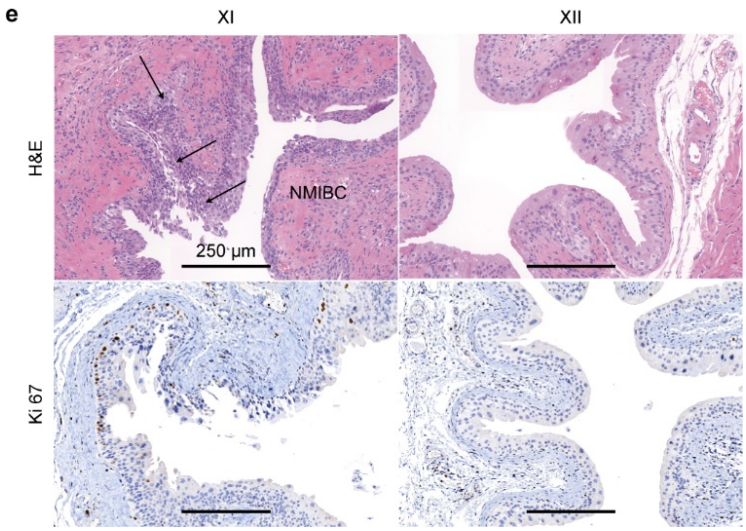
Comment 9: Presence of absence of "NMIBC signatures" is not a sufficient pathologic assessment of bladders harvested from treated mice. Instead, validated features of NMIBC as determined by H&E and IHC (Ki-67, GATA3, CK5, etc) should be assessed, ideally by a trained pathologist.

Response: We appreciate your valuable comment and have performed the suggested IHC analysis of Ki-67 on the preserved bladder tissue slices with the help of a trained pathologist, as the co-first author of Liyang Wang and the co-responding author of Dr. Guoliang Yang are full-time Ph.D. student and doctor in the Department of Urology of Renji Hospital. Meanwhile, all the rest authors have been in this field for years with abundant experience in in vivo experiments and related pathologic assessment.

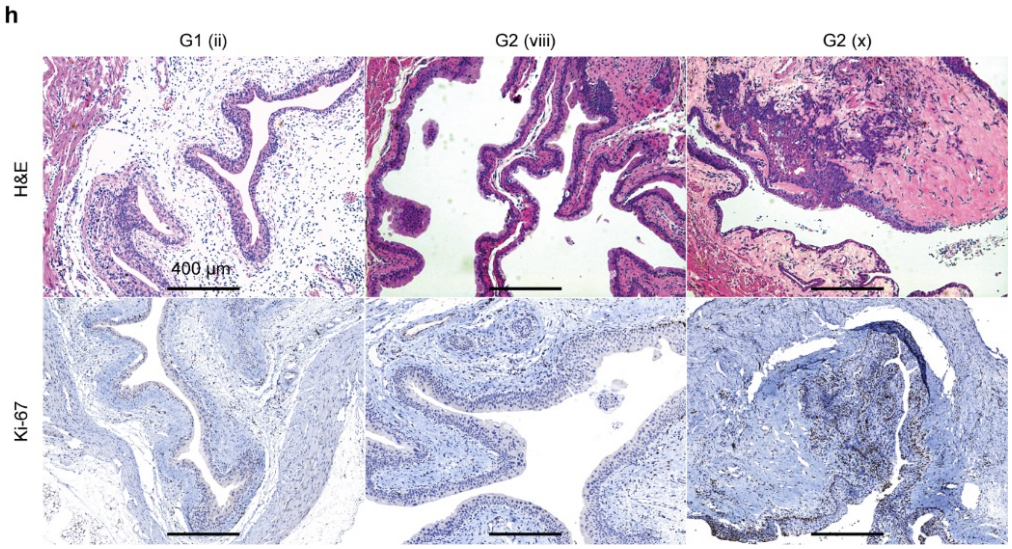
As shown in **Supplementary Figure 20**, the bladder tissues of healthy mice and mice treated with NSs-RB-F/cRGD + 6 Gy were found with the lowest expression of Ki-67, while the rest groups including 5-ALA + laser exhibited higher levels of Ki-67 expression, indicating efficient therapeutic effects of single-f-PDT at day 21. In **Figure 6d**,**e**, the mice that survived at day 56 with 5-ALA+laser were found with the presence of Ki-67 expression, while the mice with NSs-RB-F/cRGD + 6 Gy were found with low expression, the results demonstrated the robust tumour recurrence inhibition by f-PDT. In **Figure 7h**, only the mouse that died at day 35 was detected with high Ki-67 expression in contrast to all the nine survived mice at day 56. These results by Ki-67 assessment were not only in good consistency with that by H&E staining but also provided more evidence to support our conclusions. Meanwhile, we have also revised the "*NMIBC signatures*" into the more professionally used "*NMIBC histopathological features*" in the revised manuscript with more descriptions in the Method as "*The pathologic assessment of bladders was analyzed with H&E staining and Ki-67 assessment with the assistance of a trained pathologist based on the criteria of the Health/World International Society of Urological Pathology Organization*".



***New* Supplementary Figure 20** | Ki-67 staining of bladders obtained from each treatment groups.



***Revised* Figure 6 | d**,**e**, Photographs (**d**) and representative H&E and Ki-67 staining images (**e**) of bladders dissected from the remaining NMIBC mice in groups of 5-ALA+laser and NSs-RB-cRGD+6 Gy at day 56.



***Revised* Figure 7 | h**, Representative H&E and Ki-67 staining images of bladders dissected from mice in G1 and G2 at day 56 and G2(x) at day 31.

Comment 10: The immune cell analyses (Figure 5e-k) are largely descriptive and do not directly support differences in efficacy among different treatment regimens. Immune infiltration varies widely among bladder tumors and is not clearly related to tumor response in many cases. In my opinion, these immune-based analyses do not provide strong support for clinically relevant differences in activity among treatment arms.

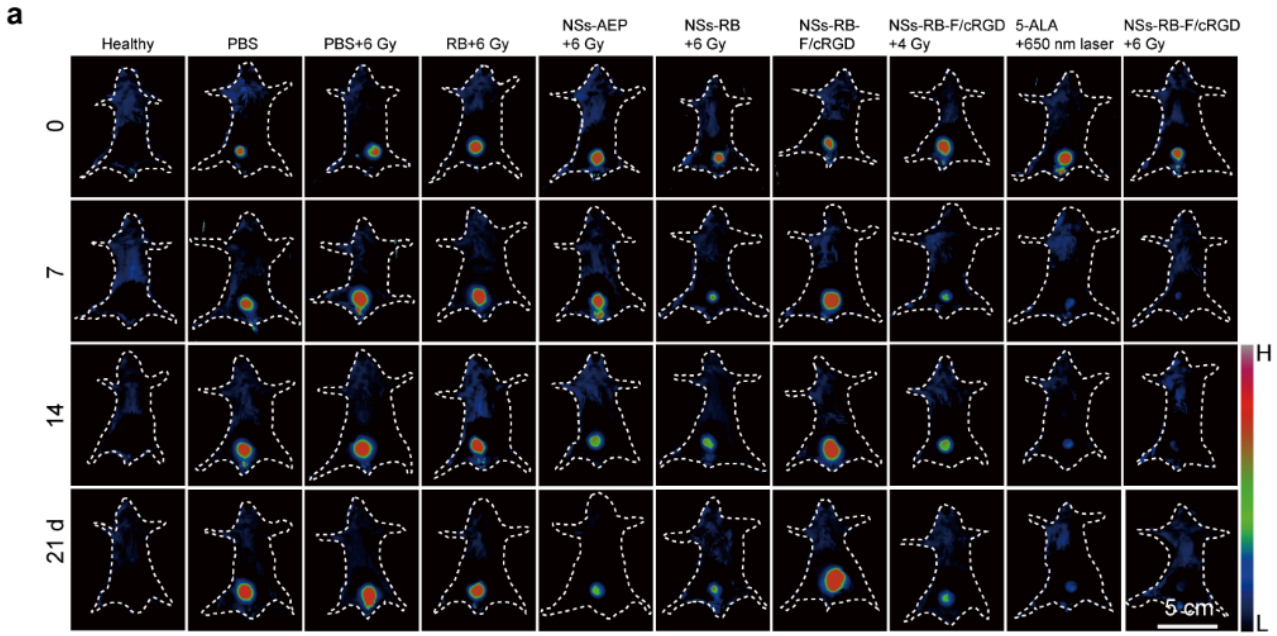
Response: We truly thank you for this valuable suggestion and information. While all the researchers have been in the field of nanomedicine for years, you may also find that we focused more on materials science with precise design and engineering of functional nanoplatform and their potential for promising imaging and therapeutic nanotechnology. The immune cell analyses (**Figure 5e-k**) were conducted as supplementary evidence following

literature (ref 50, 69-74) to exhibit the changes in bladders from mice with different treatments. Restored immune homeostasis was used according to literature based on the widely accepted German semi-quantitative scoring system. Similarly, immune cell analyses of the corresponding spleens for support in the previous manuscript.

According to your valuable suggestion, we now just provided the H&E staining images of CD4 and CD8 cell proliferation in the bladder with the widely used semi-quantitative scoring and removed the conclusion of restored immune homeostasis in the revised manuscript. We maintained the description and conclusions obtained with spleens, as they are the most important and largest immune organ (*Lancet* 2001, 357, 1777–1789; *Nat. Rev. Immunol.* 2023, 23, 705–719) and literature has demonstrated similar differences as the evidence of restored immune homeostasis.

Comment 11: In Fig 6A, would prefer to label columns with actual treatments rather than roman numerals.

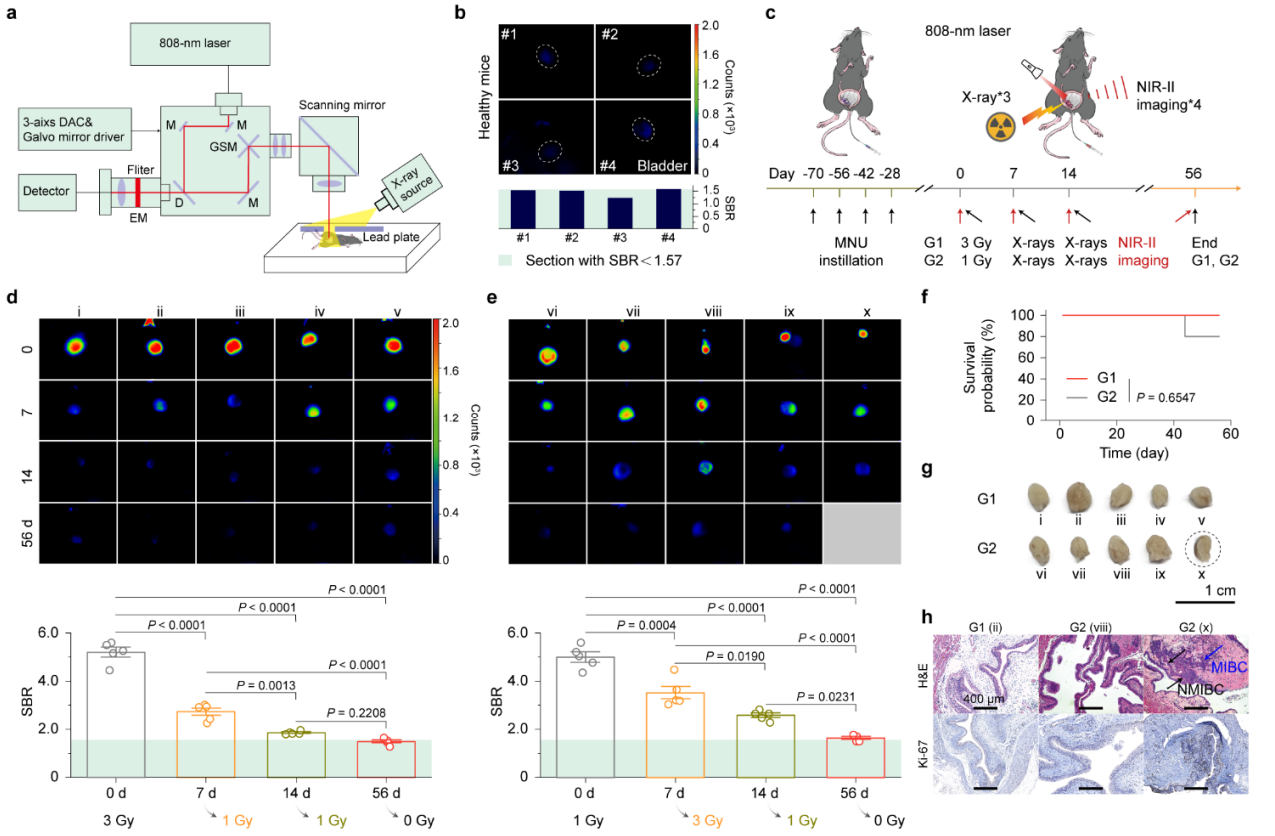
Response: We thank you for this suggestion and have added the label columns with actual treatments as suggested in **Figure 6a** and other related figures.



***Revised* Figure 6 | a**, Representative in vivo NIR-II fluorescence images of NMIBC mice from each group at days 0, 7, 14, and 21.

Comment 12: In experiments summarized in Fig 6A-C, it seems like there are opportunities for further informative analyses, such as: (1) what was the average signal intensity at the last scan before the mouse died? This would help establish relationship between signal intensity/properties and clinical disease course. (2) how much tumor was present by pathologic assessment at time of tumor death? This would help establish relationship between signal intensity and pathologic burden of disease.

Response: We really appreciate these insightful suggestions. Regarding the comment of "*the average signal intensity and the relationship between signal intensity/properties*", in fact, this was also the exact shortcomings we found in **Figure 6A-C** that the conventional small animal living imaging system failed to quantify imaging signals, as the images could only be indirectly and inaccurately analyzed with the software of ImageJ by counting the intensities of all pixels. Under this circumstance, we decided to establish the lab-made multiple-excitation fast NIR photon counter system to directly collect photon numbers of real-time NIR-II fluorescence imaging and quantify SBRs to immediately adjust the doses for the following treatment. To demonstrate the robustness of this yet unreported concept and strategies, we employed two model experiments with a relatively high dose of 3 Gy and a relatively low dose of 1 Gy to mimic two divergent clinical therapies. And all the data shown in **Figure 7** have confirmed our design and concept of a concise and intuitive tool in reflecting the relationship between signal intensity and tumour development.



***Revised* Figure 7 | a**, Scheme of our lab-made system (M: mirror; D: dichroic mirror; GSM: Galvo scanning mirror; EM: emission). **b**, In vivo NIR-II fluorescence images (top) and corresponding SBRs (bottom) of four healthy mice. **c**, Illustration of the experimental protocols for on-demand f-PDT with three fractions. **d**, In vivo NIR-II fluorescence images (top) and corresponding SBRs quantification (bottom) of all the NMIBC mice in G1 at days 0, 7, 14, and 56. **e**, In vivo NIR-II fluorescence images (top) and corresponding SBRs quantification (bottom) of all the NMIBC mice in G2 at days 0, 7, 14, and 56. **f**, Survival probability of mice in G1 and G2 for 56 days. **g**, Photographs of the bladders dissected at day 56 from all the mice in G1 and G2. **h**, Representative H&E and Ki 67 staining images of bladders dissected from mice in G1 and G2 at day 56 and G2(x) at day 31.

Regarding the comments on the "number of tumours presented by pathologic assessment" and their benefits for "establishing relationship between the signal intensity and pathologic burden of disease", we have presented the H&E staining of all the bladders from the three remaining mice treated with 5-ALA+laser and all the five remaining mice treated with NSs-RB-F/cRGD+6 Gy at day 56 in the previous manuscript and also added the corresponding suggested Ki-67 staining in the revised manuscript (Figure 6e and Supplementary Figure 26c,d). It could be found that all the staining analysis results confirmed the efficient tumour recurrence inhibiton by our proposed f-PDT and also the realiablity of NIR-II imaging for non-invasive monitoring. Nevertheless, we have to say that the pathologic assessment with either H&E or Ki-67 might not be sufficient to count all the cancerous lesions, because there existed hundreds of thousands of frozen slices (~5 μm thick) for one bladder tissue on a millimeter to centimeter scale. Although all assessments were conducted from the largest transverse section of bladder tissues with the assistance of a trained pathologist, inaccurate counting of tumour lesions in the bladder tissues, especially the small one, was inescapable and less precise to establish relationship between the signal intensity and pathologic burden of disease.

We appreciate these comments as they may further help update our lab-made system and promote our concept with more capabilities and informative analyses or clues toward the clinical disease course. While it is beyond the scope of current work as you may find that reviewer 3 commented the manuscript was already very dense and we already have more than 50 figures, we would like to include all these insightful suggestions in the Discussion of the revised manuscript following the perspective of future work with a larger number of mice or animals as "*Fourth, as most autochthonous models display significantly more heterogeneity in terms of time to tumor development and survival after developing tumors, it would be of great significance to disclose information, such as the relationship between signal intensity and pathologic burden of disease, to extend the concept of non-invasive imaging-guided f-PDT toward possible clinical disease course*."

Reviewer #5 (co-review with Reviewer #4):

I co-reviewed this manuscript with one of the reviewers who provided the listed reports. This is part of the Nature Communications initiative to facilitate training in peer review and to provide appropriate recognition for Early Career Researchers who co-review manuscripts.

Overall response: We truly thank you for your constructive suggestions and comments, as they helped us to polish and improve our manuscript.

REVIEWERS' COMMENTS

Reviewer #1 (Remarks to the Author):

The authors have answered all the questions asked by the referee.

Reviewer #2 (Remarks to the Author):

The authors did a good job of answering all my concerns in this revised version. I have no more questions.

Reviewer #4 (Remarks to the Author):

The authors have done a nice job in comprehensively addressing my comments and making requested updates to the text. I recommend publication.

Reviewer #5 (Remarks to the Author):

I co-reviewed this manuscript with one of the reviewers who provided the listed reports. This is part of the Nature Communications initiative to facilitate training in peer review and to provide appropriate recognition for Early Career Researchers who co-review manuscripts.

Peer Review File

Manuscript Title: Full-course NIR-II imaging-navigated fractionated photodynamic therapy of bladder tumours with X-ray-activated nanotransducers

Reviewer Reports:

Reviewer #1 (Remarks to the Author):

The authors have answered all the questions asked by the referee.

Reviewer #2 (Remarks to the Author):

The authors did a good job of answering all my concerns in this revised version. I have no more questions.

Reviewer #4 (Remarks to the Author):

The authors have done a nice job in comprehensively addressing my comments and making requested updates to the text. I recommend publication.

Reviewer #5 (Remarks to the Author):

I co-reviewed this manuscript with one of the reviewers who provided the listed reports. This is part of the Nature Communications initiative to facilitate training in peer review and to provide appropriate recognition for Early Career Researchers who co-review manuscripts.

Response:

Reviewer #1:

The authors have answered all the questions asked by the referee.

Response: We thank the reviewer for all the thoughtful comments and time to help improve our manuscript.

Reviewer #2:

The authors did a good job of answering all my concerns in this revised version. I have no more questions.

Response: We thank you for your valuable time and expertise in reviewing our manuscript, which have resulted in marked improvements to the manuscript.

Reviewer #4:

The authors have done a nice job in comprehensively addressing my comments and making requested updates to the text. I recommend publication.
Response: We appreciate your feedback and affirmation and also all the valuable comments to improve our manuscript.

Reviewer #5:

I co-reviewed this manuscript with one of the reviewers who provided the listed reports. This is part of the Nature Communications initiative to facilitate training in peer review and to provide appropriate recognition for Early Career Researchers who co-review manuscripts.

Response: Thank you for your time and positive feedback. We appreciate your recognition of our responses in addressing the issues.